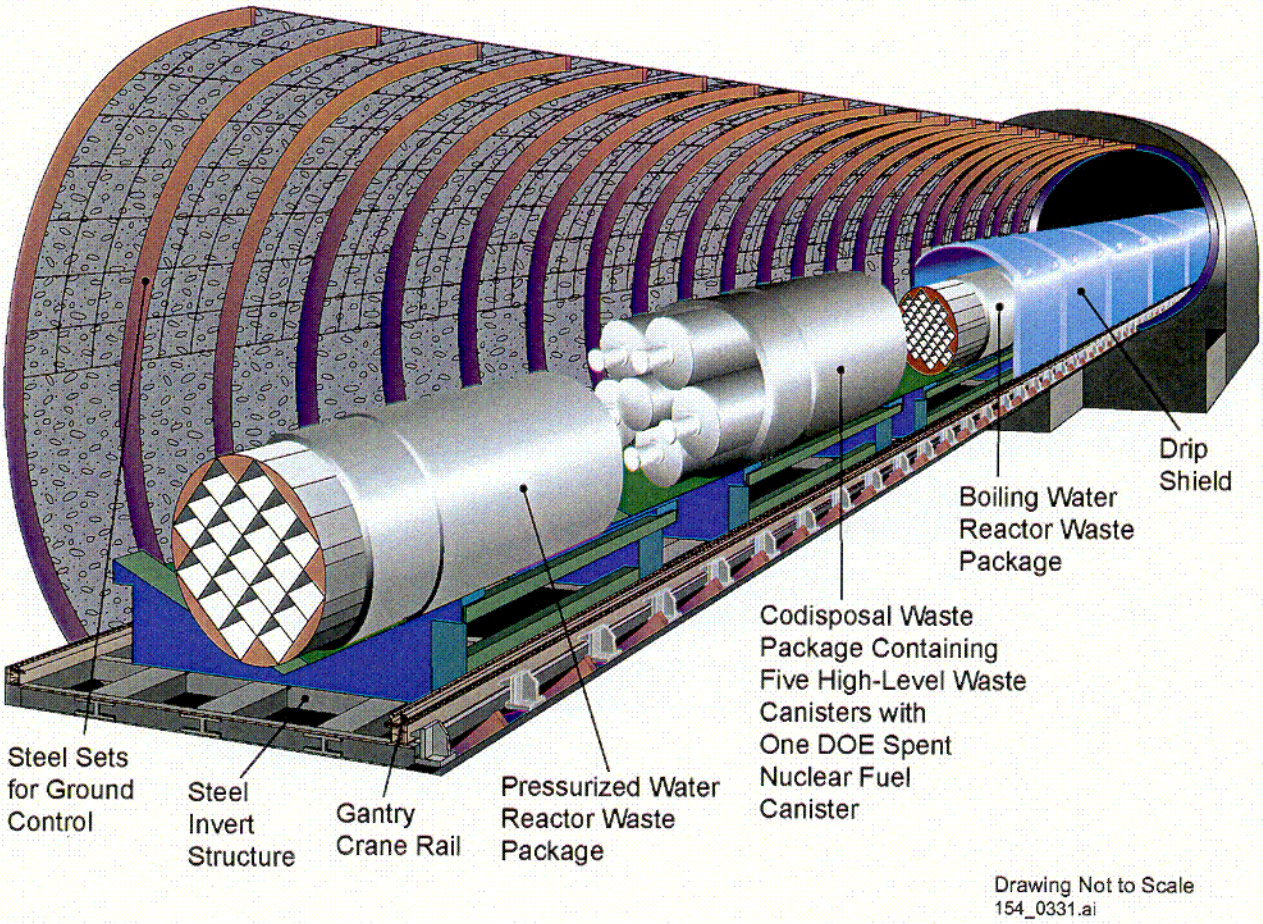

154_0331.ai

Source: CRWMS M&O 2000 [DIRS 153802], Figure 1-2.

Figure 7.1-1. Arrangements for Different Types of Waste Packages and the Drip Shield in an Emplacement Drift

C01

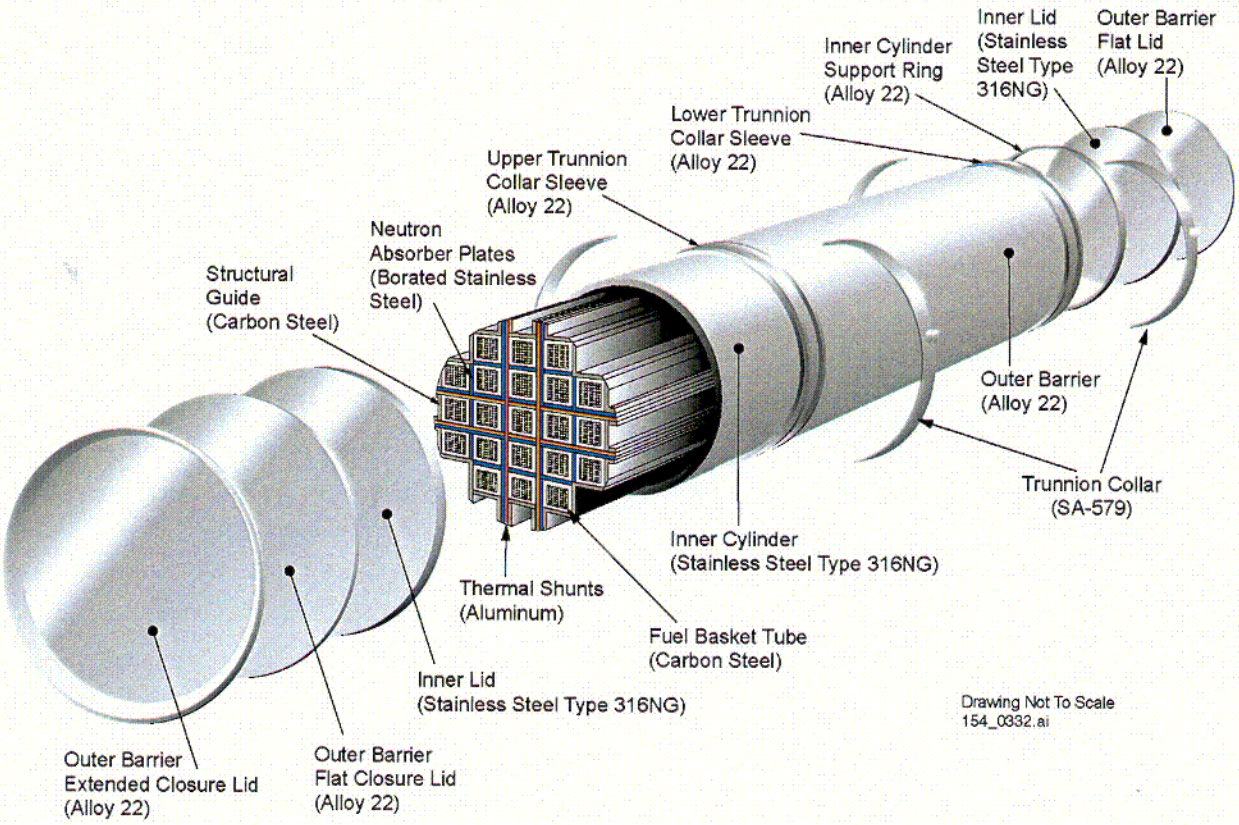

154_0332.ai

Source: CRWMS M&O 2000 [DIRS 153802], Figure 1-1.

Figure 7.1-2. Typical Waste Package Designed for 21-PWR Fuel Assemblies

C02

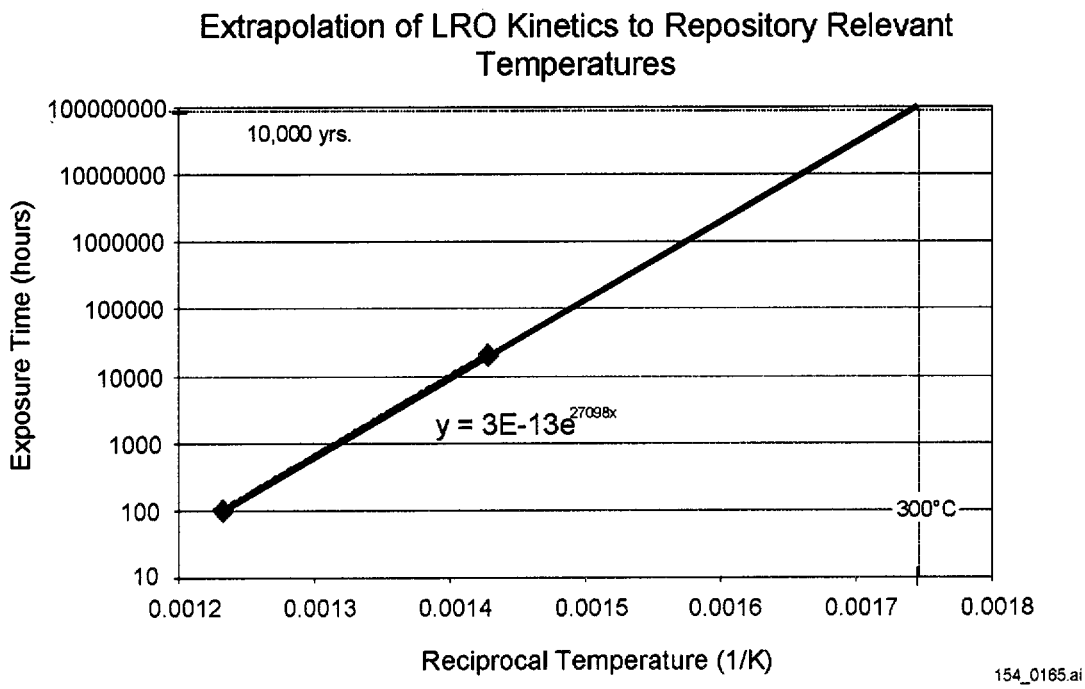

154_0165.ai

Source: Summers 2001 [DIRS 155019].

NOTE: The data in this graph correspond to aging at 538°C for 100 hours and 427°C for 20,000 hours.

Figure 7.3.2-1. Graphical Extrapolation of the Kinetic Data for Long-Range Ordering in Alloy 22 Base Metal

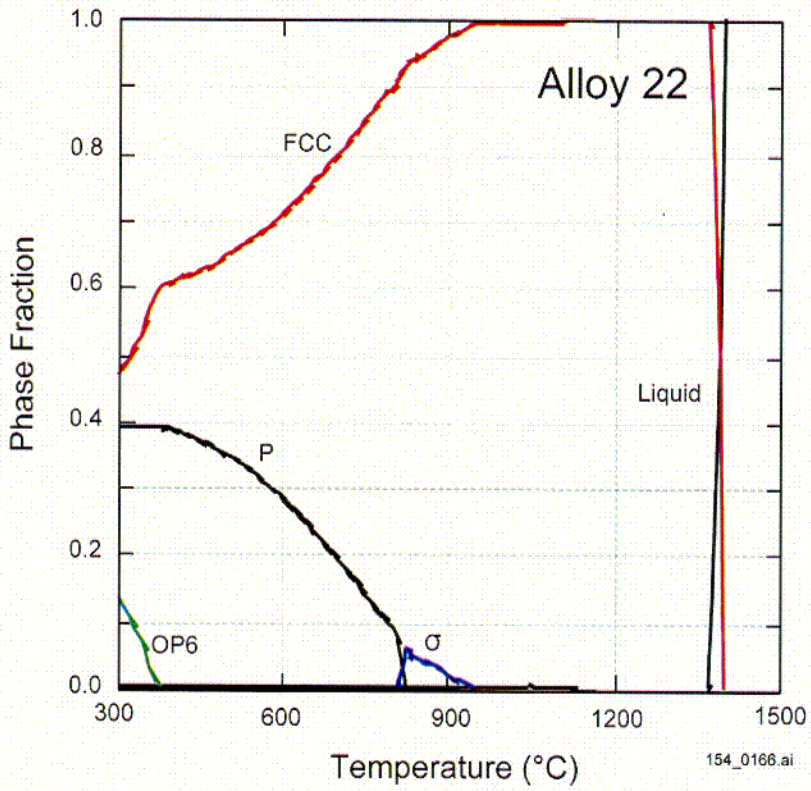

154_0166.ai

Source: Turchi 2001 [DIRS 154934].

NOTE: The calculation assumes a composition (weight percent) of 21.2 Cr-13.5 Mo-4 Fe-3 W-2 Co-0.5 Mn-0.3 V-0.08 Si-0.01 C-bal. Ni, which is typical for Alloy 22. At low temperatures, three phases are predicted to be thermodynamically stable: OP6 (which refers to the ordered phase), P, and the FCC solid solution phase. μ and P phases are similar and are not treated separately here. Sigma (σ) phase is only stable at higher temperatures.

Figure 7.3.2-2. Phase Fraction Predicted for Alloy 22 as a Function of Temperature

C03

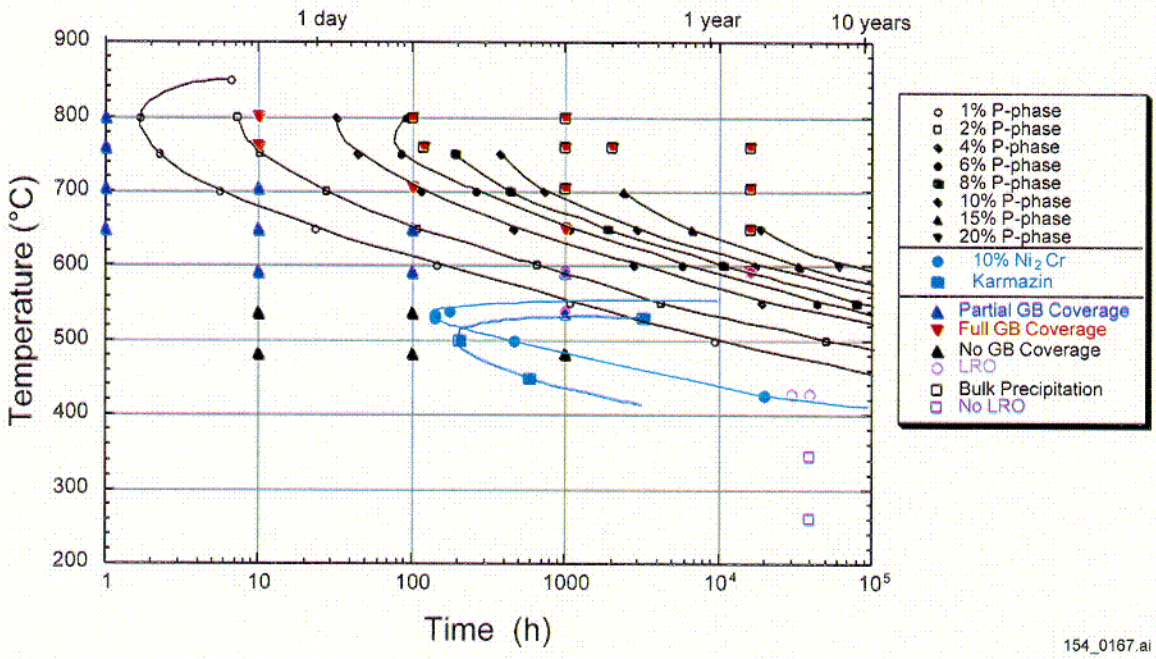

154_0167.ai

Source: Turchi 2001 [DIRS 154934].

NOTE: Lower curves describe the prediction and the results extracted from the work of Karmazin (1982). The binary alloy assumes that 10 percent of the matrix transforms into the ordered phase of Ni_2Cr-type. The ternary alloy (surrogate of Alloy 22 with 55.7 Ni-21.1 Cr-13.5 Mo in weight percent) assumes to transform into the P phase, with the transformation rate ranging from 1 to 20 percent. GB = grain boundary; LRO = long range ordering.

Figure 7.3.2-3. Isothermal Time-Temperature-Transformation Diagrams for an FCC-Based Matrix of a Binary Nickel-Chromium Alloy and a Ternary Nickel-Chromium-Molybdenum Alloy

C04

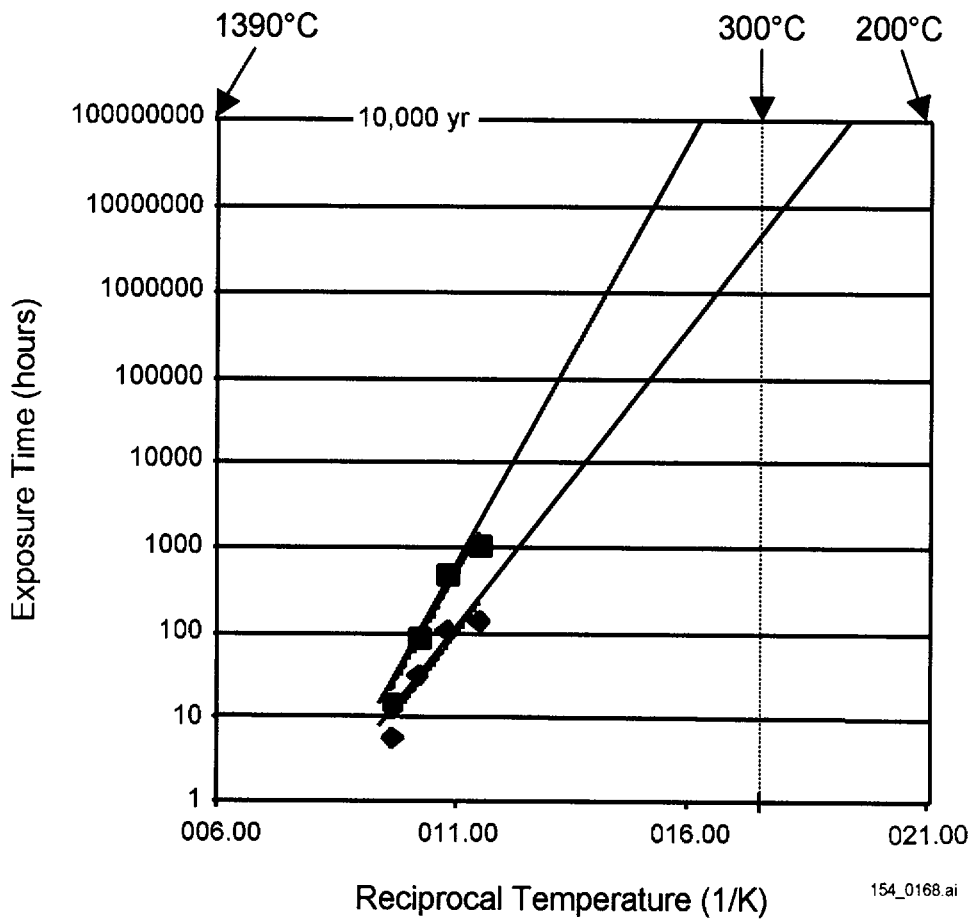

154_0168.ai

Source: Summers 2001 [DIRS 155018].

NOTE: Extrapolation of these data indicate that further nucleation and growth of the phases that form during welding of Alloy 22 is possible in 10,000 years at temperatures between 200 and 300°C and higher.

Figure 7.3.2-4. Extrapolation of Volume Fraction Data from Half-Inch Thick, Alloy 22, Double-V, Gas-Tungsten-Arc Welds

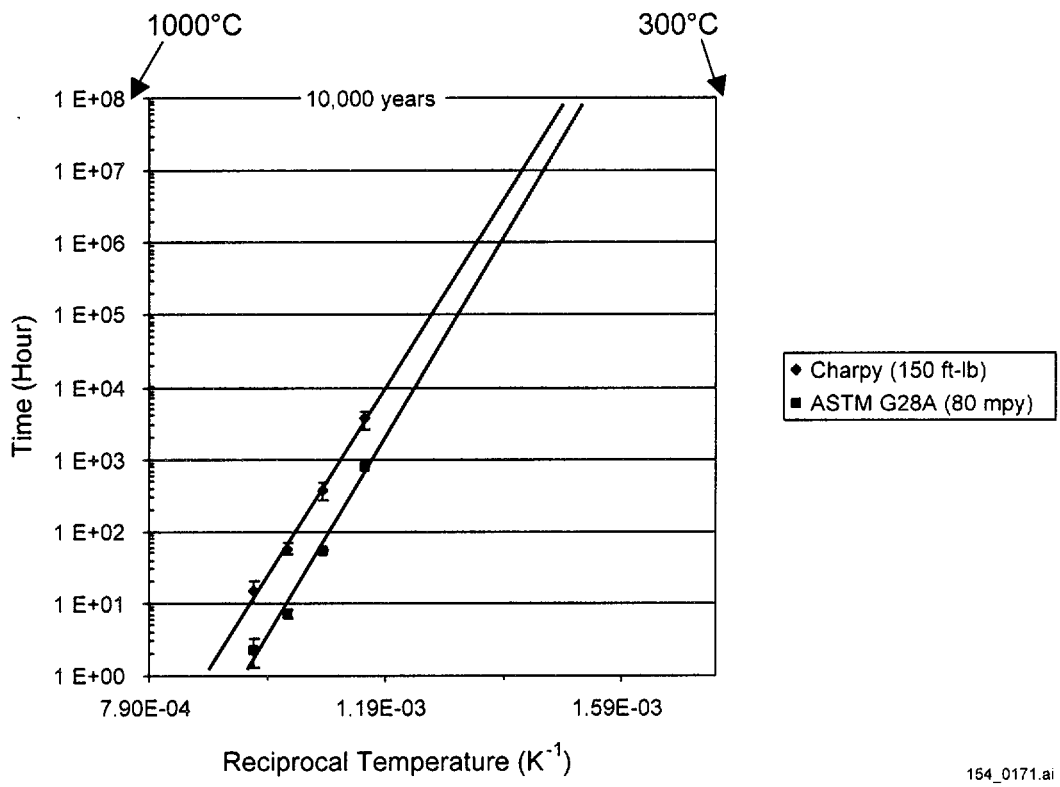

154_0171.ai

Source: Rebak et al. 2000 [DIRS 146910]; G 28-97 1997 [DIRS 154712].

Figure 7.3.2-5. Extrapolation of Mechanical (Charpy Impact Toughness) and Electrochemical (Corrosion Resistance) Behavior of Alloy 22

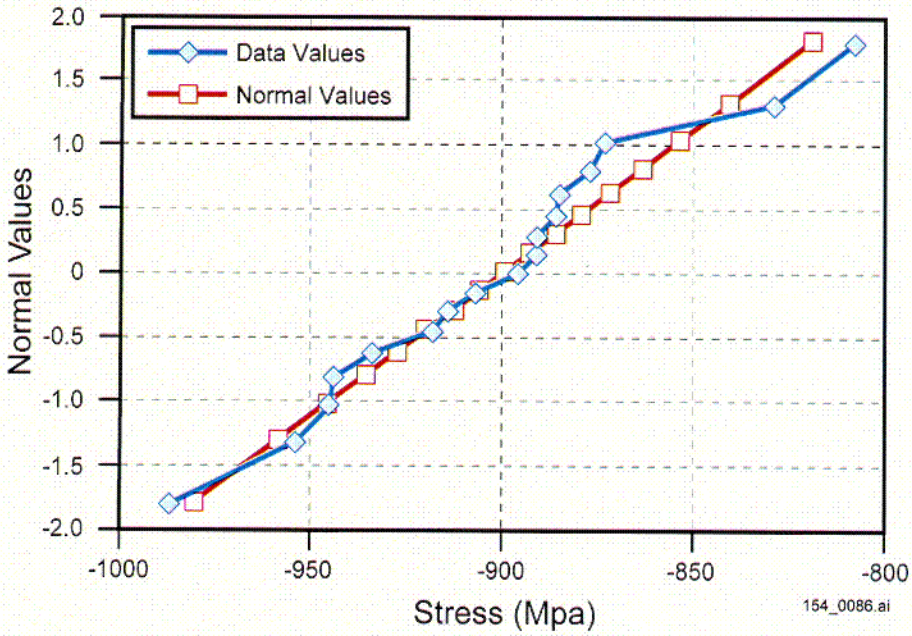

154_0086.ai

Source: Bullard 2001 [DIRS 155035].

Figure 7.3.3-1. Fractile Plot of Measured Surface Residual Stress Values for Shot Peened-Incoloy 908 Samples

C05

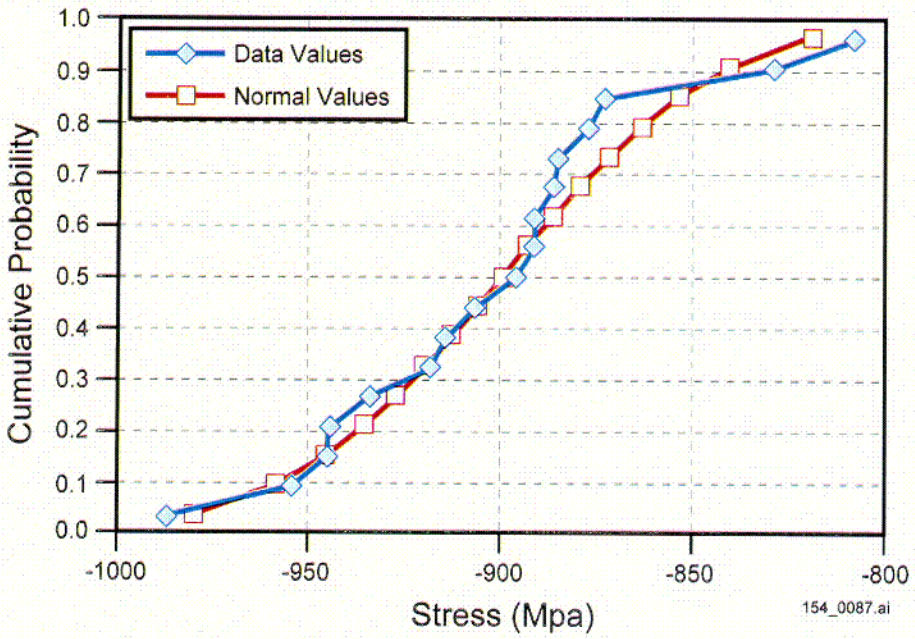

154_0087.ai

Source: Bullard 2001 [DIRS 155035].

Figure 7.3.3-2. Probability Plot of Measured Surface Residual Stress Values for Shot Peened Incoloy 908 Samples

C04

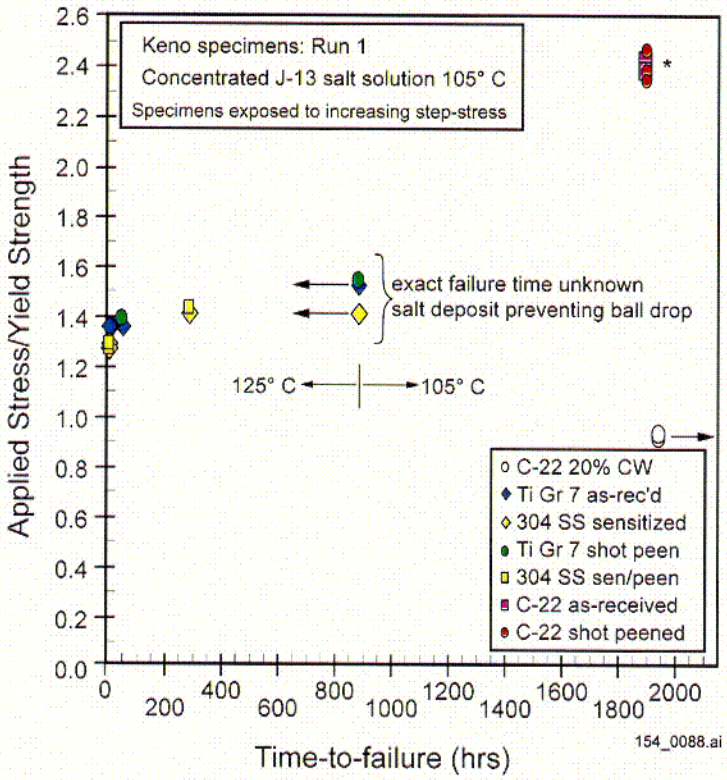

154_0088.ai

Source: Pasupathi 2001 [DIRS 154936].

NOTE: Test used basic saturated water (approximately 5500-fold well J-13 water, pH = 12.4).

Figure 7.3.3-3. Constant Load (Uniaxial Tension) Stress Corrosion Crack Initiation Test No. 1

C07

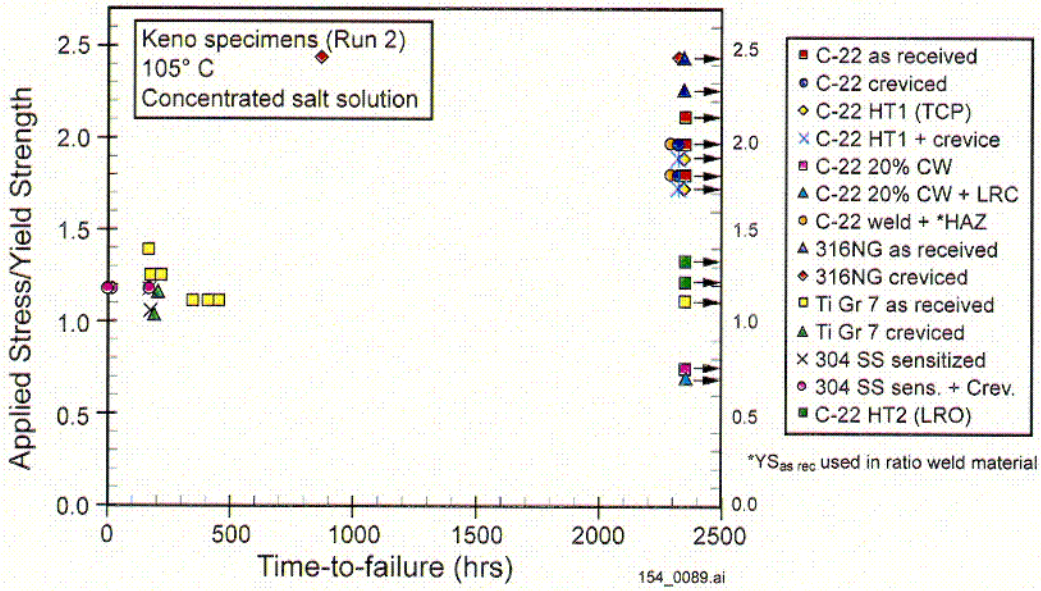

12-4-00 1:30 pm 1000 psi = time zero; 0 hr
12-11-00 2:00 pm 1500 psi; leak followed in the am; 168.5 hr
12-12-00 7:00 am pressure reduced; autoclave off; 185.5 hr
12-20-00 3:11 pm pressure 1249 psi; 185.5 hr
123-21-00 7:00 am pressure 1400 psi; 201.3 hr
12-21-00 3:20 pm pressure 1500 psi; 209.65 hr
3-20-01 11:00 am t = 2341.3; 40 failures to date; 121 unfailed specimens remain

154_0089.ai

Source: Pasupathi 2001 [DIRS 154936].

NOTE: Test used Basic Saturated Water (approximately 5500-fold well J-13 water, pH = 12.4).

Figure 7.3.3-4. Constant Load (Uniaxial Tension) Stress Corrosion Crack Initiation Test No. 2

C08

Metal	Barrier Oxide Layer	Outer Layer/Solution

1. $m + V_M^{\chi'} \xrightarrow{k_1} M_M + v_m + \chi e'$
2. $m \xrightarrow{k_2} M_i^{\chi+} + v_m + \chi e'$
3. $m \xrightarrow{k_3} M_M + (\chi/2)V_O^{\bullet\bullet} + \chi e'$
4. $M_M \xrightarrow{k_4} M^{\delta+} + V_M^{\chi'} + (\delta - \chi)e'$
5. $M_i^{\chi+} \xrightarrow{k_5} M^{\delta+} + (\delta - \chi)e'$
6. $V_O^{\bullet\bullet} + H_2O \xrightarrow{k_6} O_O + 2H^+$
7. $MO_{\chi/2} + \chi H^+ \xrightarrow{k_7} M^{\delta+} + (\chi/2)H_2O + (\delta - \chi)e'$

154_0132.ai

154_0132.ai

Source: Macdonald 2001 [DIRS 154736], pp. 18 to 22.

NOTE: m = metal atom, M_M = metal cation in cation site, O_O = oxygen ion in anion site, $M_i^{\chi+}$ = cation interstitial, $V_M^{\chi'}$ = cation vacancy, and $V_O^{\bullet\bullet}$ = oxygen vacancy, and v_m = vacancy in metal phase.

Figure 7.3.4-1. Elementary Interfacial Reactions Postulated in the Point Defect Model to Generate or Annihilate Point Defects in the Barrier Layer of a Passive Film

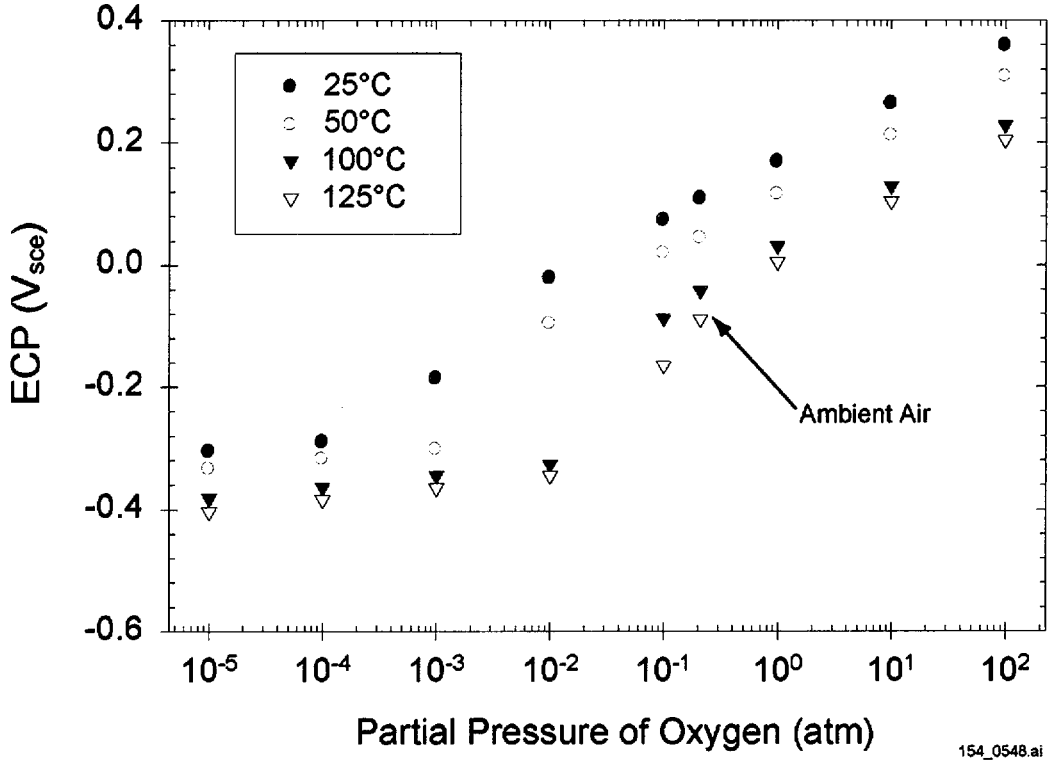

154_0548.ai

Source: Macdonald 2001 [DIRS 154736], pp. 18 to 22.

NOTE: Parameter values assumed in the analysis: pH = 3, saturated NaCl solution, electrolyte film thickness = 0.01 cm. SCE = saturated calomel electrode.

Figure 7.3.4-2. Dependence of Electrochemical Corrosion Potential on the Partial Pressure of Oxygen and on Temperature

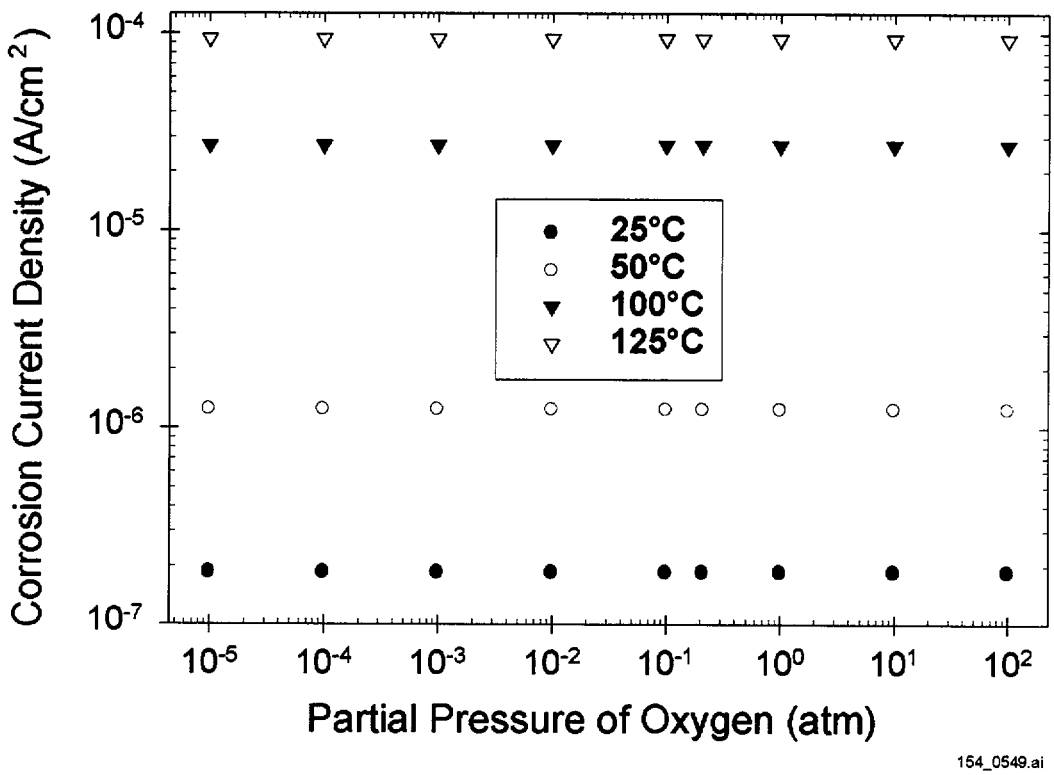

154_0549.ai

Source: Macdonald 2001 [DIRS 154736], pp. 18 to 22.

NOTE: Parameter values assumed in the analysis: pH = 3, saturated NaCl solution, electrolyte film thickness = 0.01 cm.

Figure 7.3.4-3. Corrosion Current Density as a Function of the Partial Pressure of Oxygen and Temperature

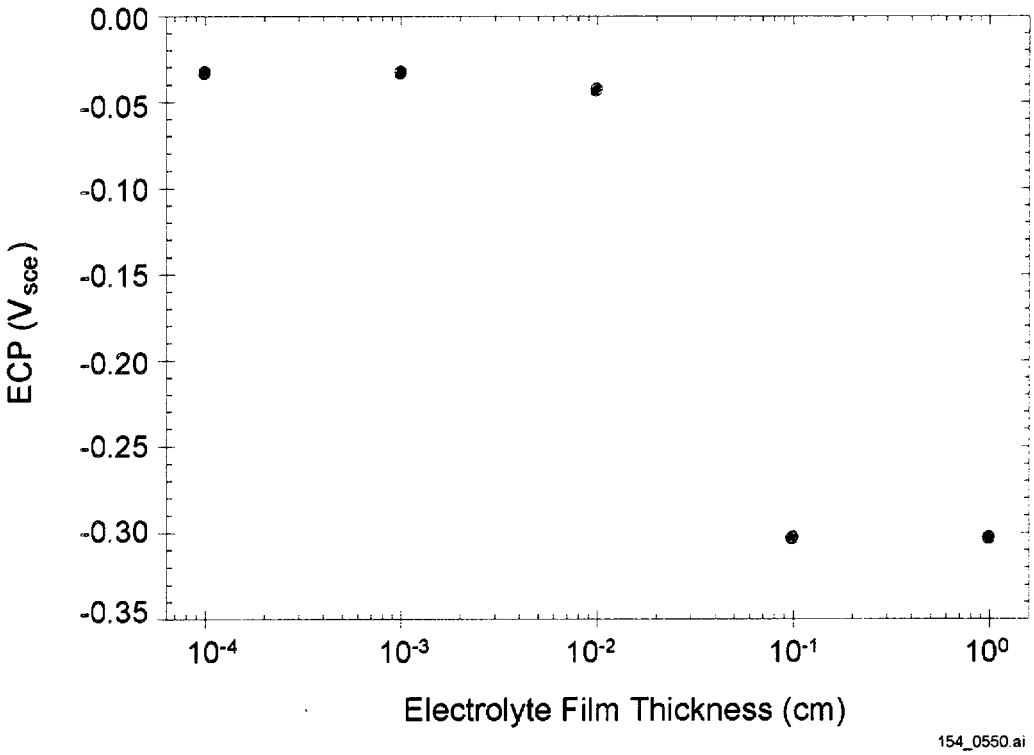

154_0550.ai

Source: Macdonald 2001 [DIRS 154736], pp. 18 to 22.

NOTE: Parameter values assumed in the analysis: T=100°C, pH = 3, oxygen partial pressure = 0.21 atm, saturated NaCl solution. SCE = saturated calomel electrode.

Figure 7.3.4-4. Calculated Electrochemical Corrosion Potential Versus Thickness of the Electrolyte Film on the Metal Surface

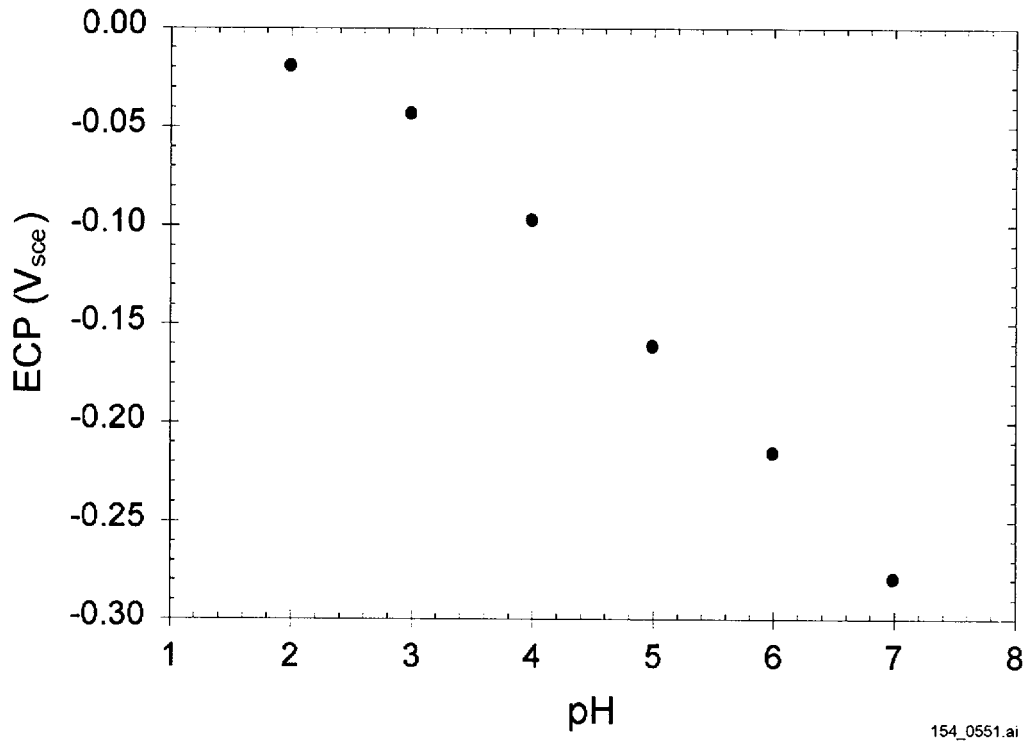

154_0551.ai

Source: Macdonald 2001 [DIRS 154736], pp. 18 to 22.

NOTE: Parameter values assumed in the analysis: T = 100°C, oxygen partial pressure = 0.21 atm, saturated NaCl solution, electrolyte film thickness = 0.01 cm. SCE = saturated calomel electrode.

Figure 7.3.4-5. Calculated Electrochemical Corrosion Potential Versus pH of the Thin Electrolyte Film on the Alloy Surface

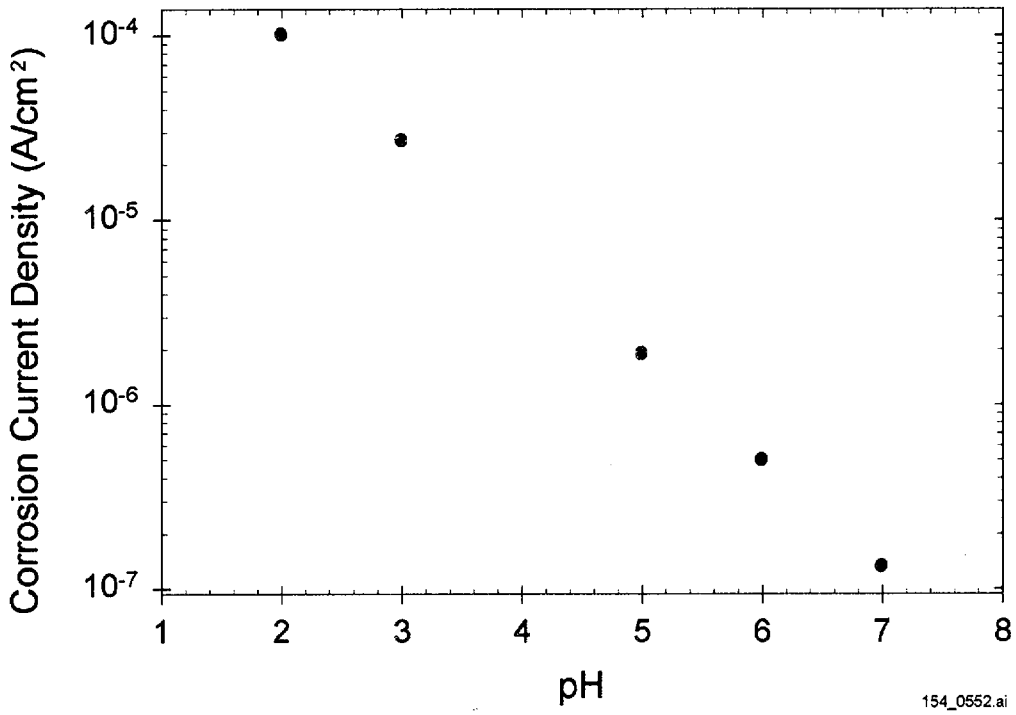

154_0552.ai

Source: Macdonald 2001 [DIRS 154736], pp. 18 to 22.

NOTE: Parameter values assumed in the analysis: T = 100°C, oxygen partial pressure = 0.21 atm, saturated NaCl solution, electrolyte film thickness = 0.01 cm.

Figure 7.3.4-6. Calculated Corrosion Current Density Versus pH of the Thin Electrolyte Film on the Alloy Surface

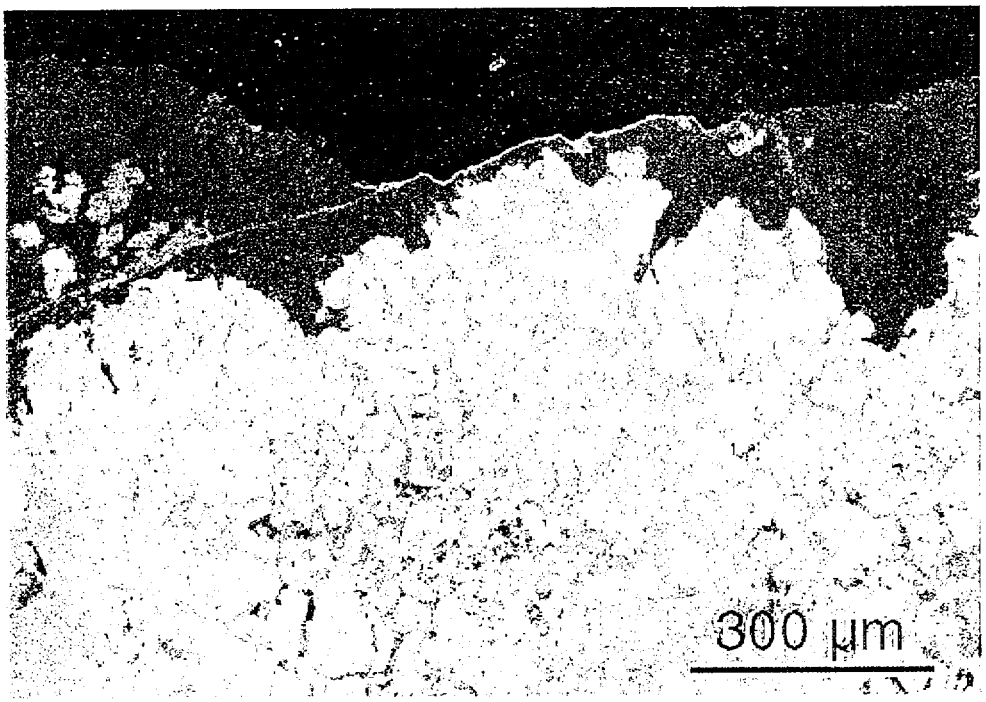

154_0138.ai

154_0138.ai

Source: Summers 2001 [DIRS 155017].

NOTE: The outer layers consist primarily of a magnesium silicate, presumably serpentine (darkest outer layer), and an iron oxide, presumably magnetite (darker gray regions). The interior of the sample is a mixture of many nonmetallic minerals and the Fe-Ni metal (brighter regions).

Figure 7.3.4-7. Mineral Variations Shown in a Scanning Electron Microscope Micrograph of a Cross Section of a Josephinite Sample

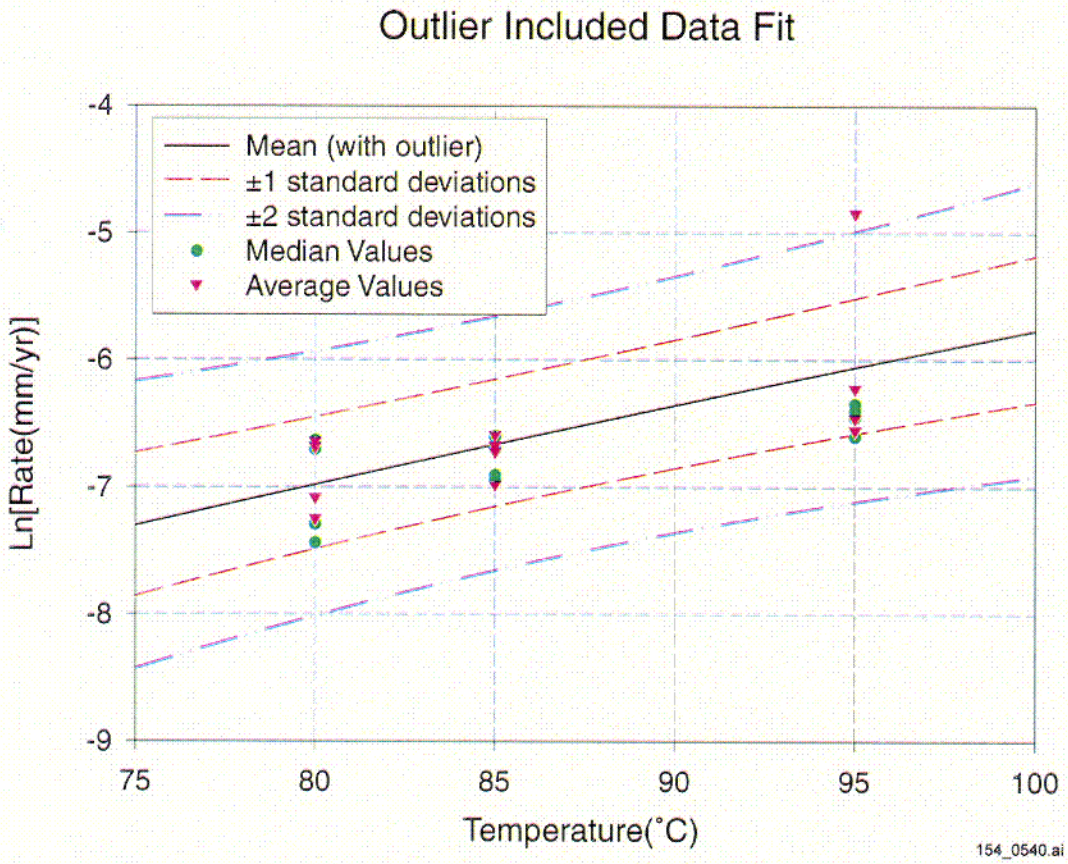

154_0540.ai

Source: Bullard 2001 [DIRS 155034].

NOTE: The data are used to evaluate the temperature dependence term only. The rate data are not used to determine the general corrosion rate values for the model.

Figure 7.3.5-1. Data Fit for Temperature Dependence of Alloy 22 General Corrosion Model I Using the Entire Data Set

C09

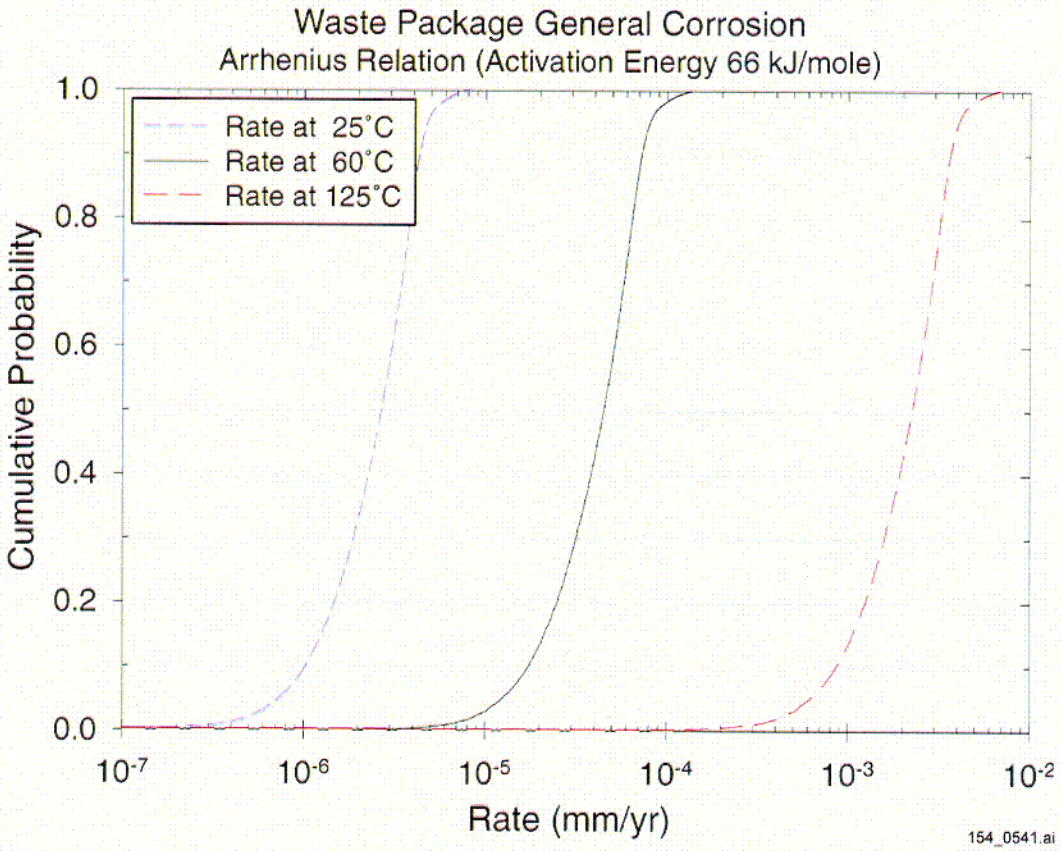

154_0541.ai

Source: Bullard 2001 [DIRS 155034].

Figure 7.3.5-2. Cumulative Distribution Functions of General Corrosion Rate of the Waste Package Outer Barrier at 25, 60, and 125°C Calculated with Temperature-Dependent Alloy 22 General Corrosion Model I

C10

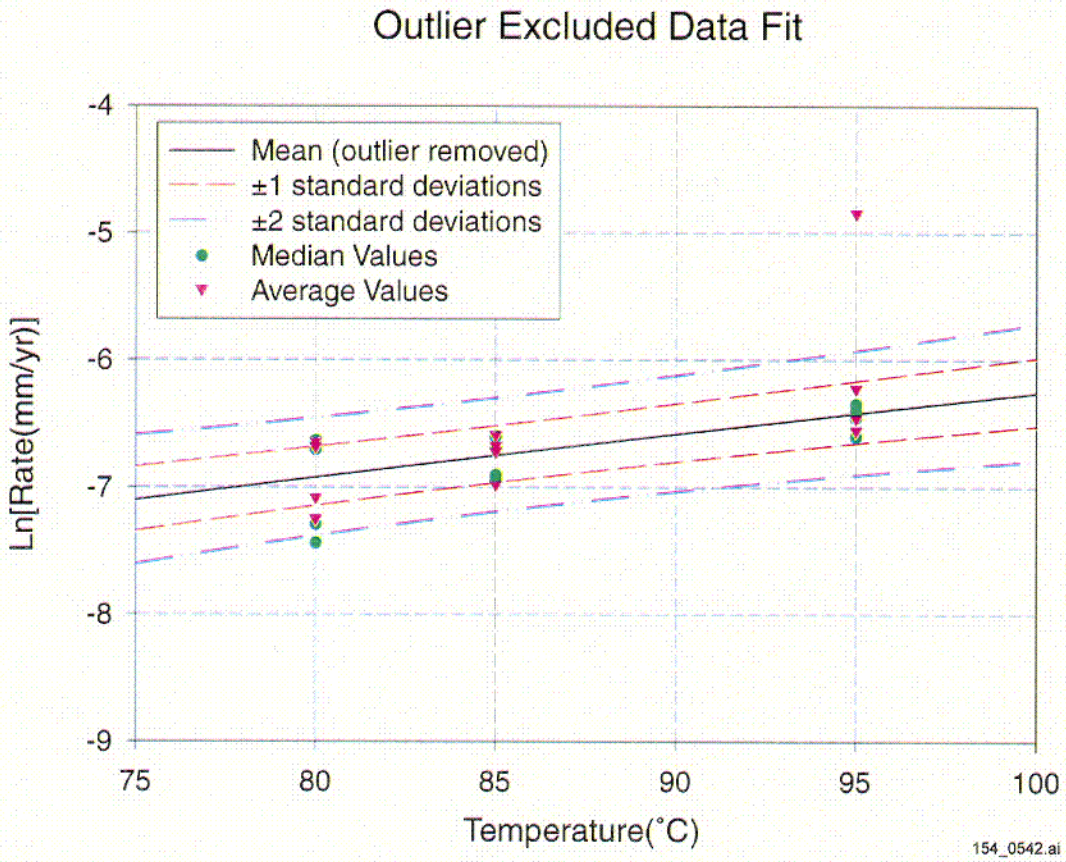

154_0542.ai

Source: Bullard 2001 [DIRS 155034].

NOTE: The data are used to evaluate the temperature-dependent term only. The rate data are not used to determine the general corrosion rate values for the model.

Figure 7.3.5-3. Data Fit for Temperature Dependence of Alloy 22 General Corrosion Model II with the Outer Excluded

C11

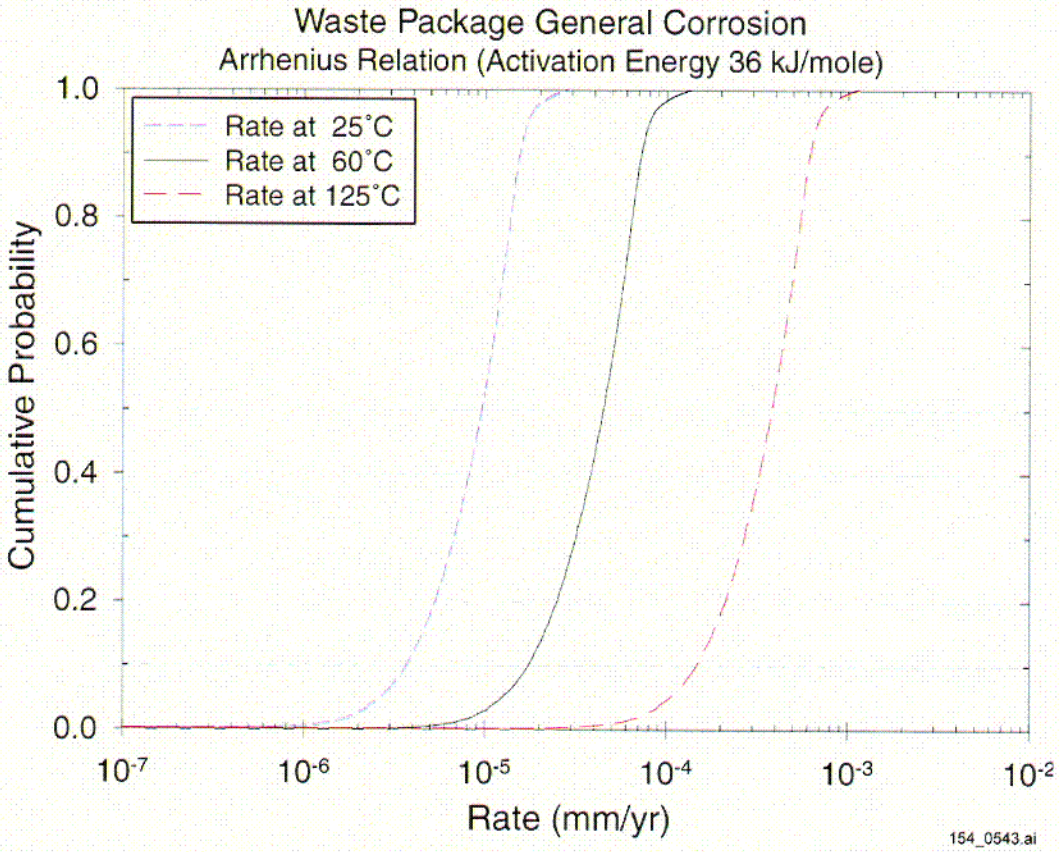

154_0543.ai

Source: Bullard 2001 [DIRS 155034].

Figure 7.3.5-4. Cumulative Distribution Functions of General Corrosion Rate of the Waste Package Outer Barrier at 25°, 60°, and 125°C Calculated with Temperature-Dependent Alloy 22 General Corrosion Model II

C12

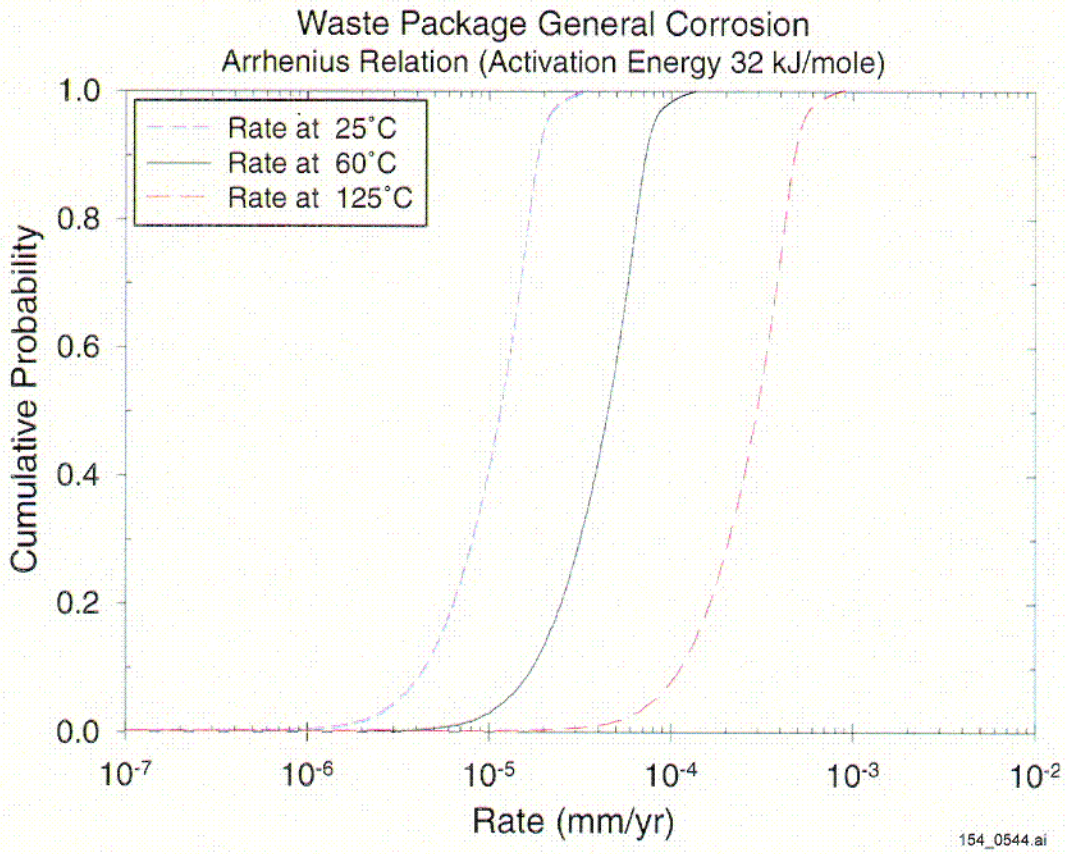

154_0544.ai

Source: Bullard 2001 [DIRS 155034].

Figure 7.3.5-5. Cumulative Distribution Functions of General Corrosion Rate of the Waste Package Outer Barrier at 25, 60, and 125°C Calculated with Temperature-Dependent Alloy 22 General Corrosion Model III

C13

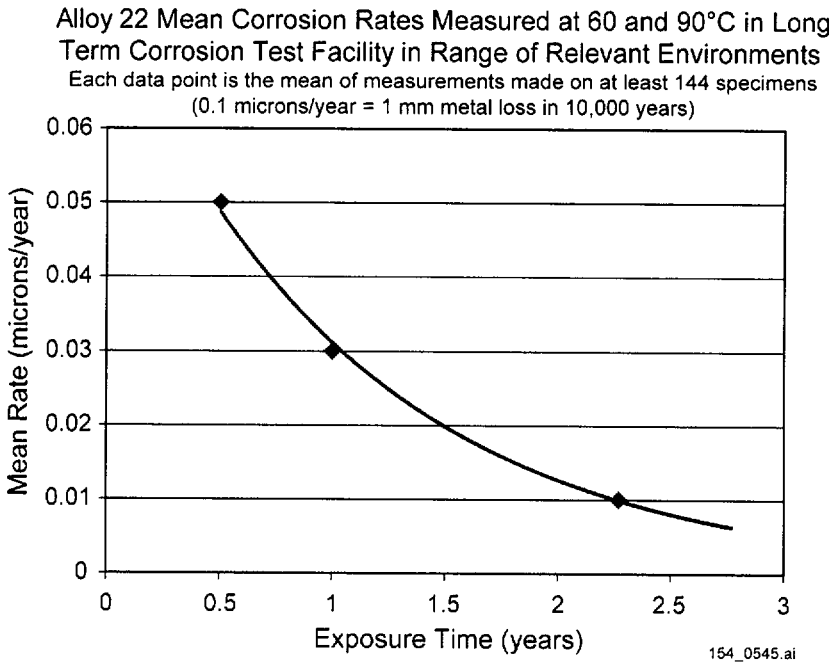

154_0545.ai

Source: Bullard 2001 [DIRS 155034].

Figure 7.3.5-6. Mean General Corrosion Rate of Alloy 22 Versus Exposure Time for Weight Loss Specimens from the Long-Term Corrosion Testing Facility

FIGURE REMOVED

Figure 7.3.5-7

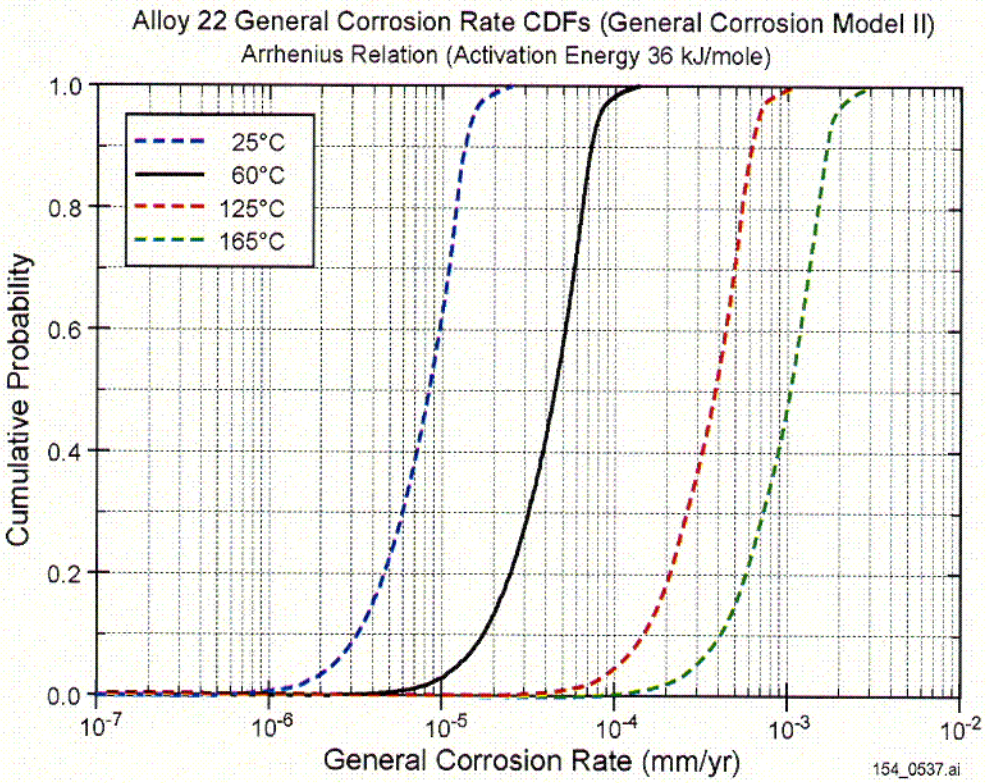

154_0537.ai

Source: Mon 2001 [DIRS 155202].

NOTE: Cumulative distribution functions of general corrosion rate of the Alloy 22 waste package outer barrier at 25, 60, 125, and 165°C with temperature-dependent Alloy 22 general corrosion model II.

Figure 7.3.5-8. Cumulative Distribution Functions of General Corrosion Rate of the Alloy 22 Waste Package Outer Barrier

C14

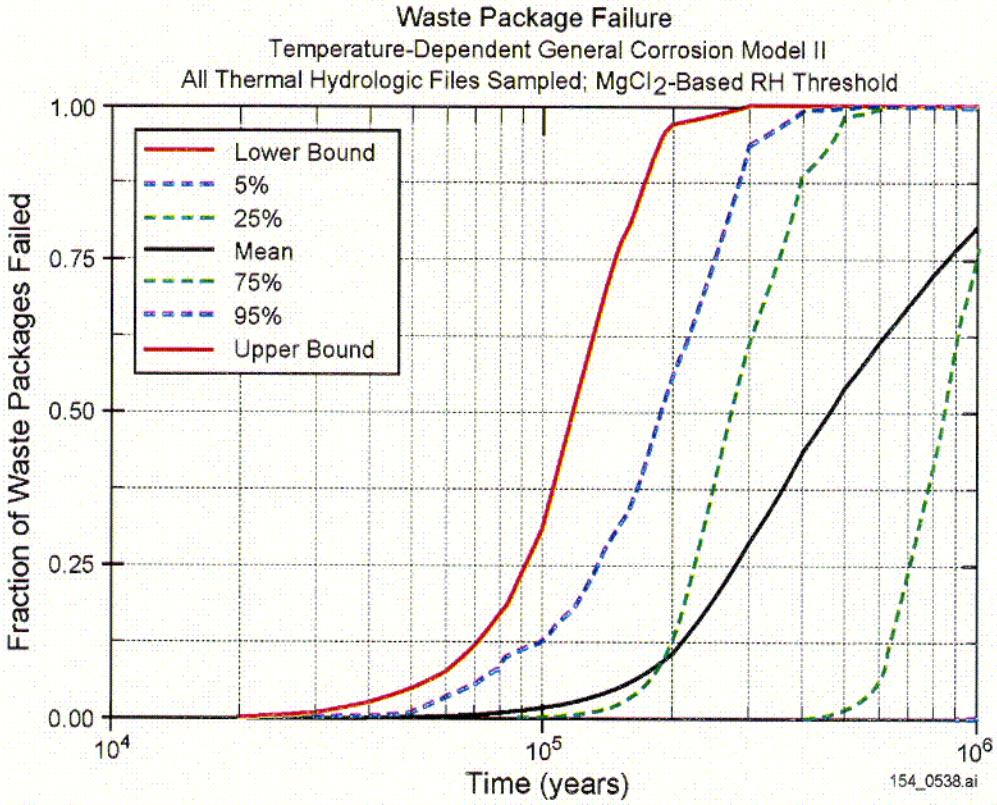

154_0538.ai

Source: Mon 2001 [DIRS 155202].

NOTE: Waste package failure profile with time incorporating the temperature-dependent Alloy 22 general corrosion model II and using a critical relative humidity function based on $MgCl_2$ deliquescence points. Shown are the upper bound, mean, and 95th, 75th and 25th percentile confidence intervals of the failure (first breach) profile of waste packages with time. The analysis assumes 100 percent uncertainty in the general corrosion rates for the Alloy 22 waste package outer barrier. The relative humidity and temperature histories of the waste packages and drip shields included in the analysis are sampled from the temperature and relative humidity histories for the entire repository.

Figure 7.3.5-9 Waste Package Failure Profile with Time Incorporating the Temperature-Dependent Alloy 22 General Corrosion Model II

C15

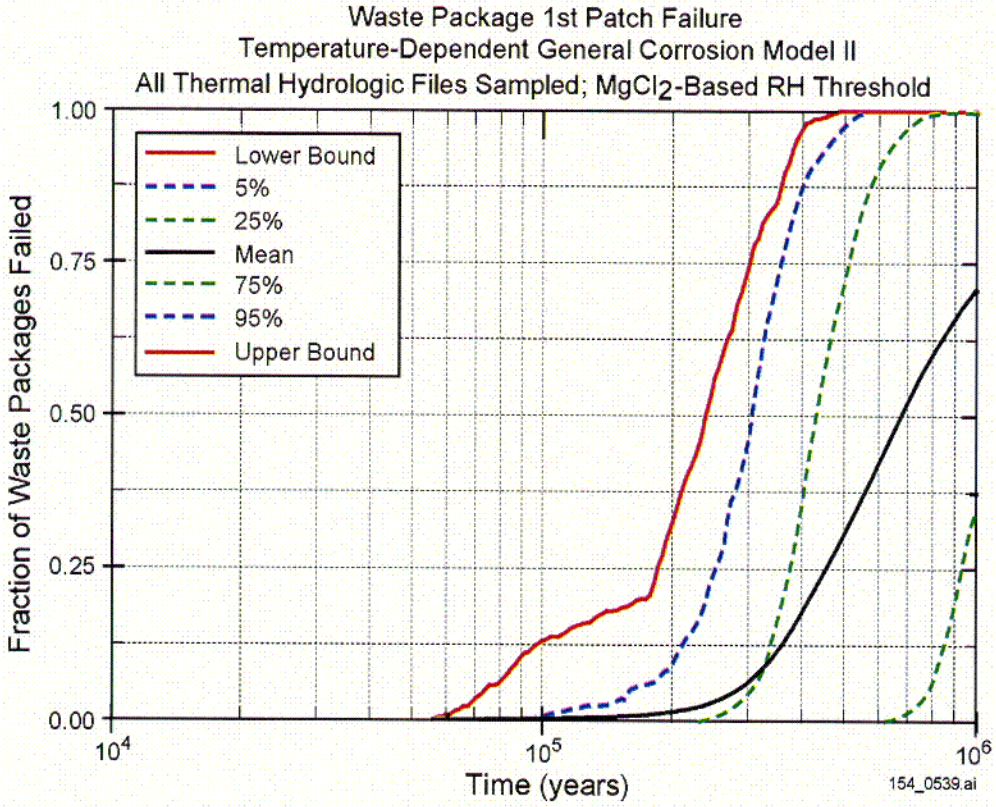

154_0539.ai

Source: Mon 2001 [DIRS 155202].

NOTE: Waste package first patch breach profile with time incorporating the temperature-dependent Alloy 22 general corrosion model II and using a critical relative humidity function based on $MgCl_2$ deliquescence points. Shown are the upper bound, mean, and 95th, 75th and 25th percentile confidence intervals of the failure (first breach) profile of waste packages with time. The analysis assumes 100 percent uncertainty in the general corrosion rates for the Alloy 22 waste package outer barrier. The relative humidity and temperature histories of the waste packages and drip shields included in the analysis are sampled from the temperature and relative humidity histories for the entire repository.

Figure 7.3.5-10 Waste Package First Patch Breach Profile with Time Incorporating the Temperature-Dependent Alloy 22 General Corrosion Model II

C16

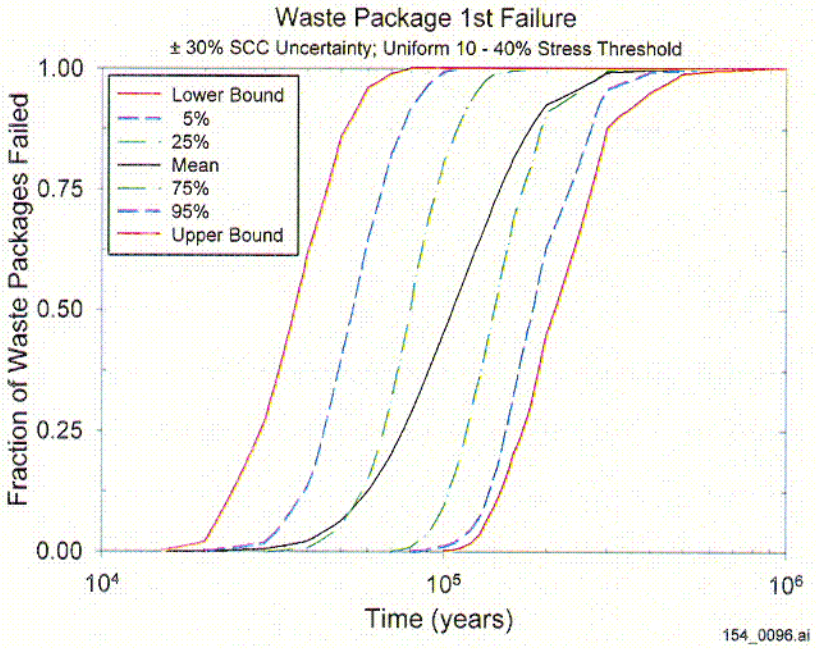

154_0096.ai

Source: Mon 2001 [DIRS 154872].

NOTE: Shown in the figure are the upper and lower bounds, mean, and 95th, 75th, 25th and 5th percentile confidence intervals of the first breach (failure) profile of waste packages with time. SCC = stress corrosion cracking.

Figure 7.4-1. Waste Package Failure over Time for the Baseline WAPDEG Model

C17

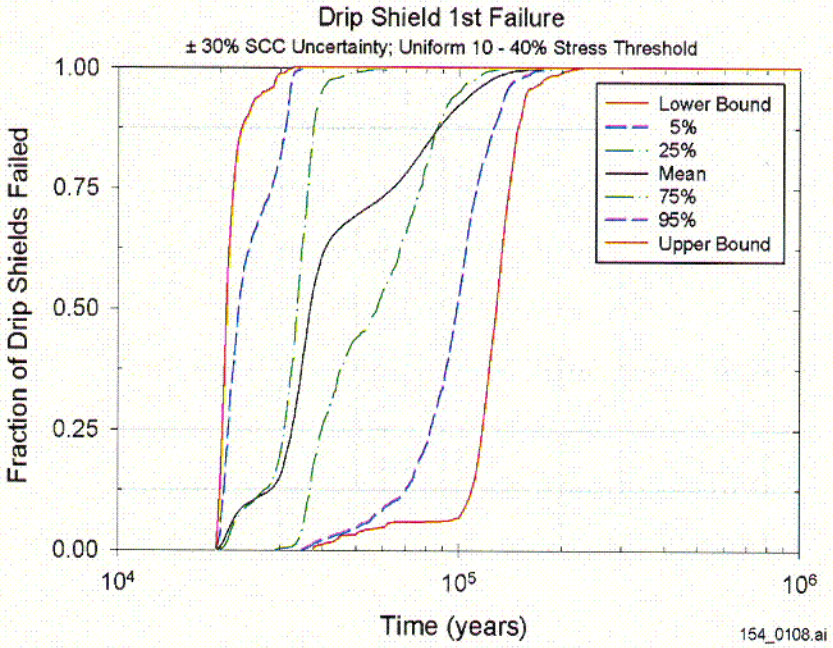

154_0108.ai

Source: Mon 2001 [DIRS 154872].

NOTE: Shown in the figure are the upper and lower bounds, mean, and 95th, 75th, 25th and 5th percentile confidence intervals of the first breach (failure) profile of drip shields with time. SSC = stress corrosion cracking.

Figure 7.4-2. Drip Shield Failure over Time for the Baseline WAPDEG Model

C18

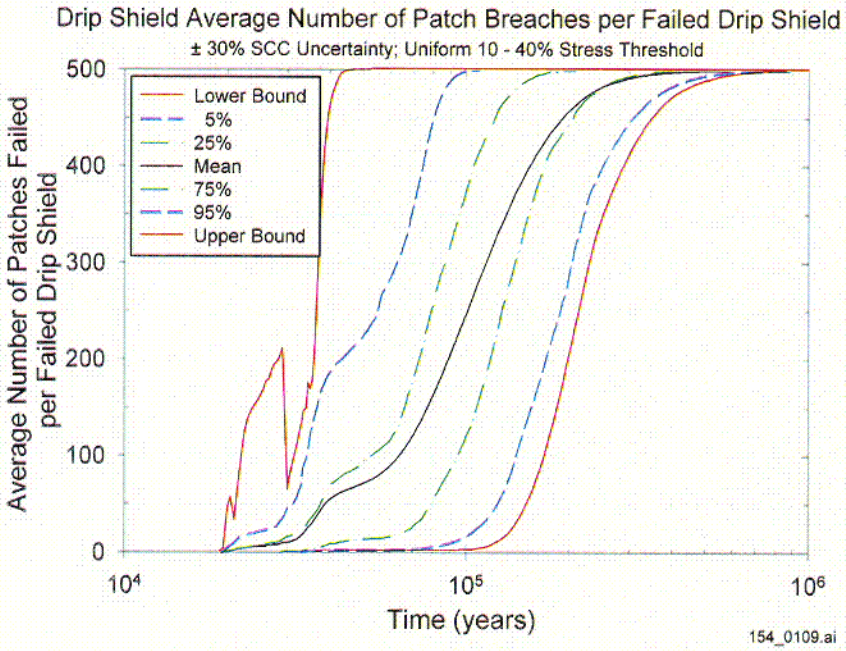

154_0109.ai

Source: Mon 2001 [DIRS 154872].

NOTE: Shown in the figure are the upper and lower bounds, mean, and 95th, 75th, 25th and 5th percentile confidence intervals of the average number of drip shield patch breaches per failed drip shield with time. SSC = stress corrosion cracking.

Figure 7.4-3. Average Number of Drip Shield Patch Breaches per Failed Drip Shield for the Baseline WAPDEG Model

C19

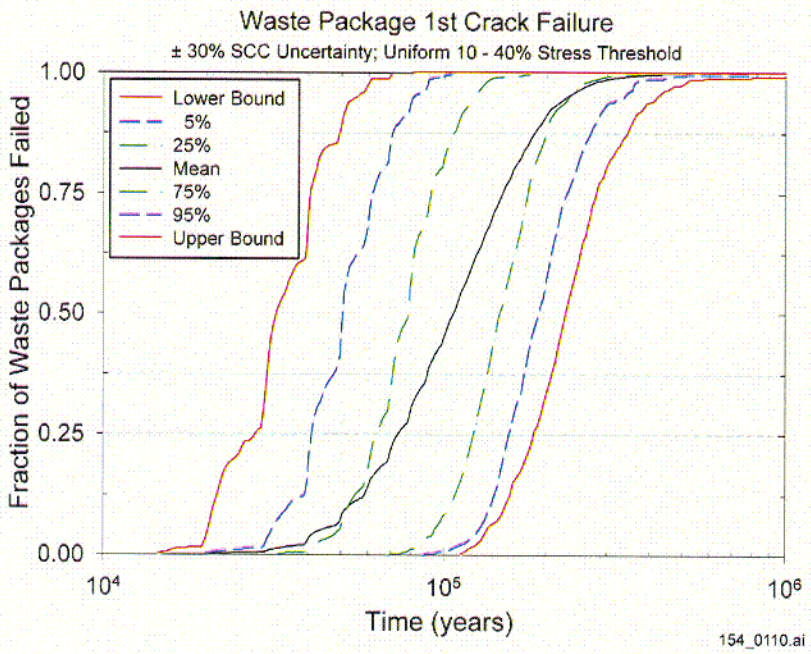

154_0110.ai

Source: Mon 2001 [DIRS 154872].

NOTE: Shown in the figure are the upper and lower bounds, mean, and 95th, 75th, 25th and 5th percentile confidence intervals of the first crack failure of waste packages with time. SSC = stress corrosion cracking.

Figure 7.4-4. Waste Package First Crack Failure for the Baseline WAPDEG Model

C20

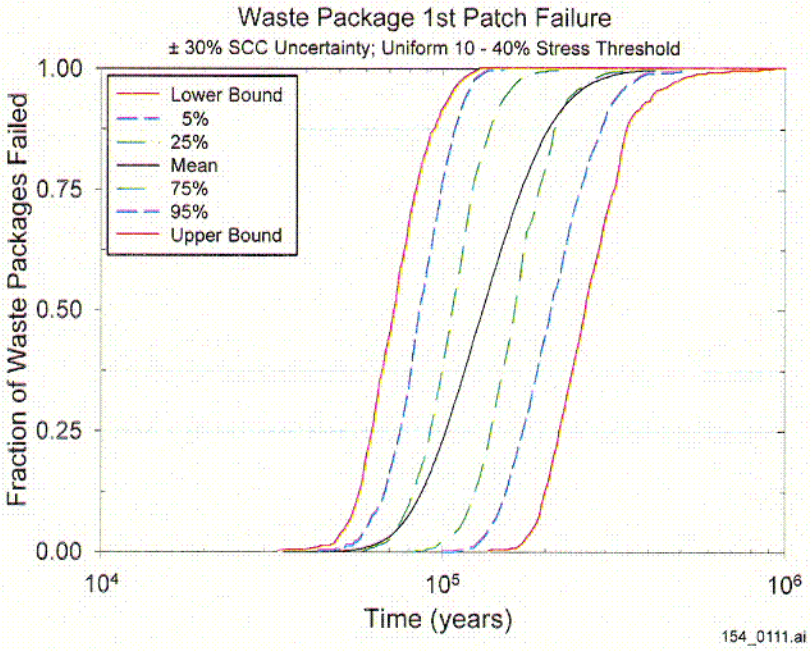

154_0111.ai

Source: Mon 2001 [DIRS 154872].

NOTE: Shown in the figure are the upper and lower bounds, mean, and 95th, 75th, 25th and 5th percentile confidence intervals of the first patch failure of waste packages with time. SSC = stress corrosion cracking.

Figure 7.4-5. Waste Package First Patch Failure for the Baseline WAPDEG Model

C21

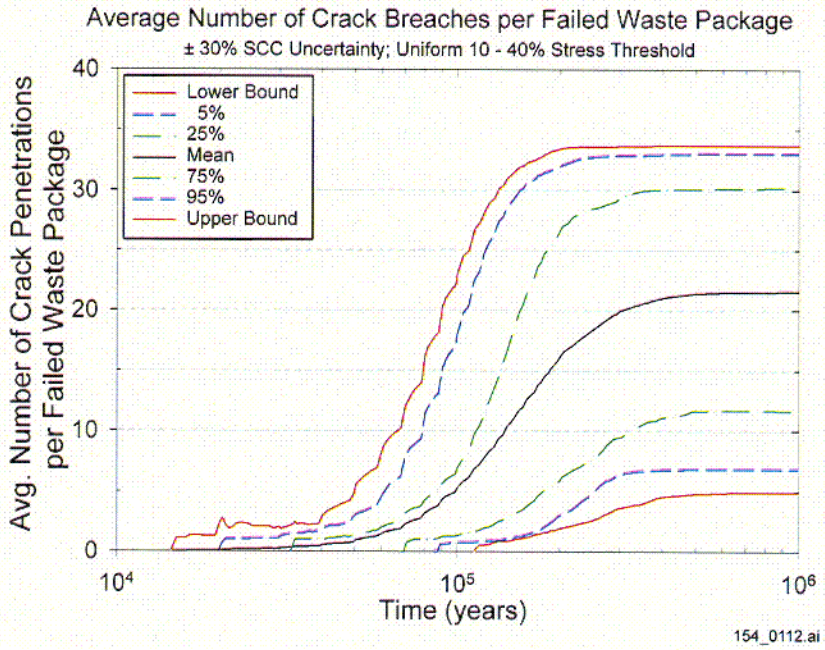

154_0112.ai

Source: Mon 2001 [DIRS 154872].

NOTE: Shown in the figure are the upper and lower bounds, mean, and 95th, 75th, 25th and 5th percentile confidence intervals of the average number of crack breaches per failed waste package with time. SSC = stress corrosion cracking.

Figure 7.4-6. Average Number of Crack Breaches per Failed Waste Package for the Baseline WAPDEG Model

C22

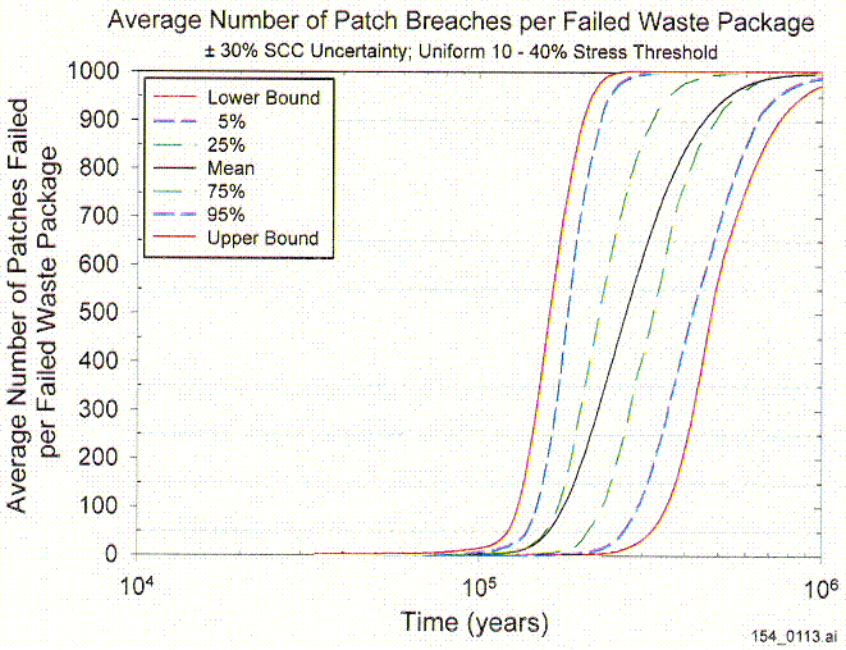

154_0113.ai

Source: Mon 2001 [DIRS 154872].

NOTE: Shown in the figure are the upper and lower bounds, mean, and 95th, 75th, 25th and 5th percentile confidence intervals of the average number of patch breaches per failed waste package with time. SSC = stress corrosion cracking.

Figure 7.4-7. Average Number of Patch Breaches per Failed Waste Package for the Baseline WAPDEG Model

C23

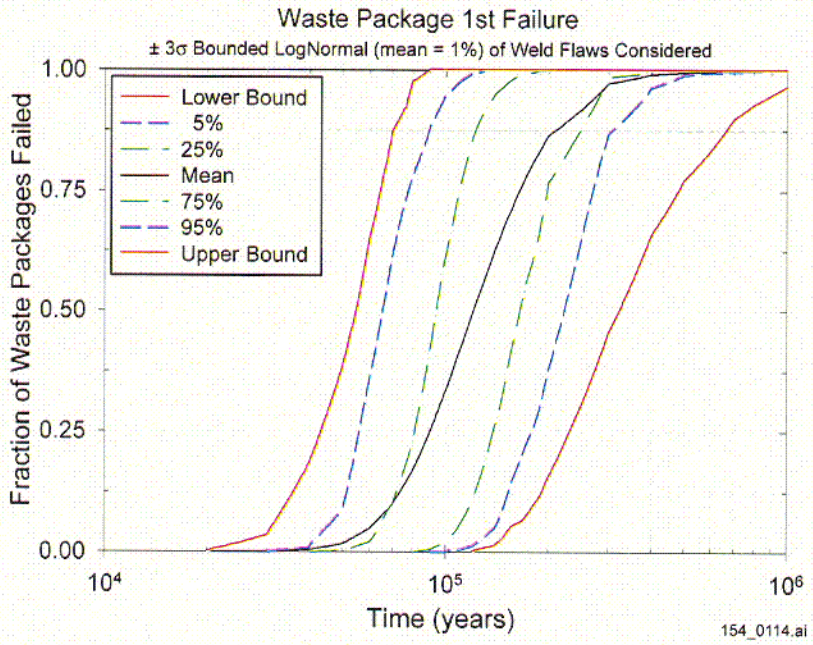

154_0114.ai

Source: Mon 2001 [DIRS 154872].

NOTE: Shown in the figure are the upper and lower bounds, mean, and 95th, 75th, 25th and 5th percentile confidence intervals of the first breach (failure) profile of waste packages with time. The fraction of weld flaws capable of propagation is sampled from a log-normal distribution with a mean of 0.01 and bounded by +3 standard deviations at 0.5 and –3 standard deviations at 0.0002.

Figure 7.4-8. Waste Package Failure with Time Incorporating the Updated Uncertainty for Weld Flaw Orientation

C24

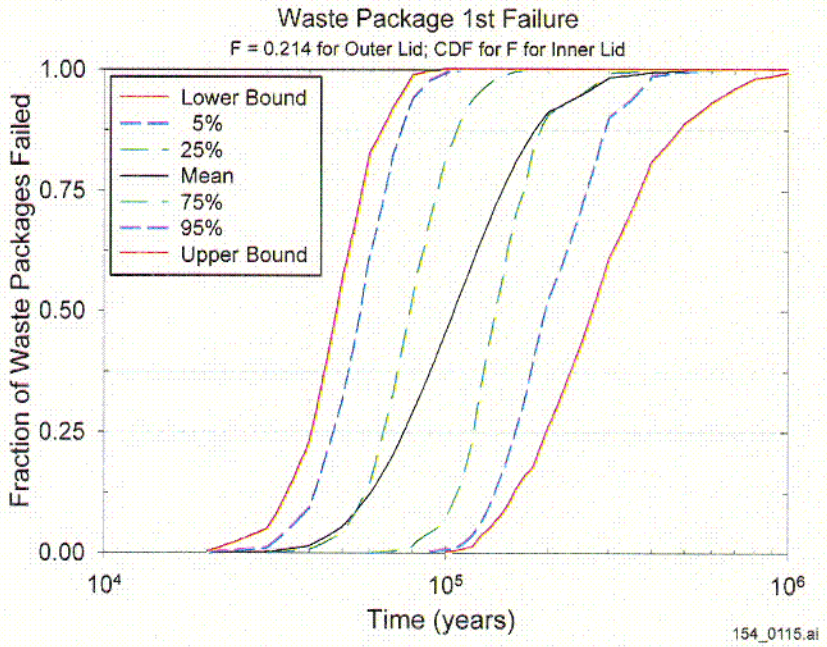

154_0115.ai

Source: Mon 2001 [DIRS 154872].

NOTE: Shown in the figure are the upper and lower bounds, mean, and 95th, 75th, 25th and 5th percentile confidence intervals of the first breach (failure) profile of waste packages with time.

Figure 7.4-9. Waste Package Failure with Time Incorporating the Updated Stress Uncertainty Bounds for the Outer and Inner Closure-Lids of the Waste Package Outer Barrier

C25

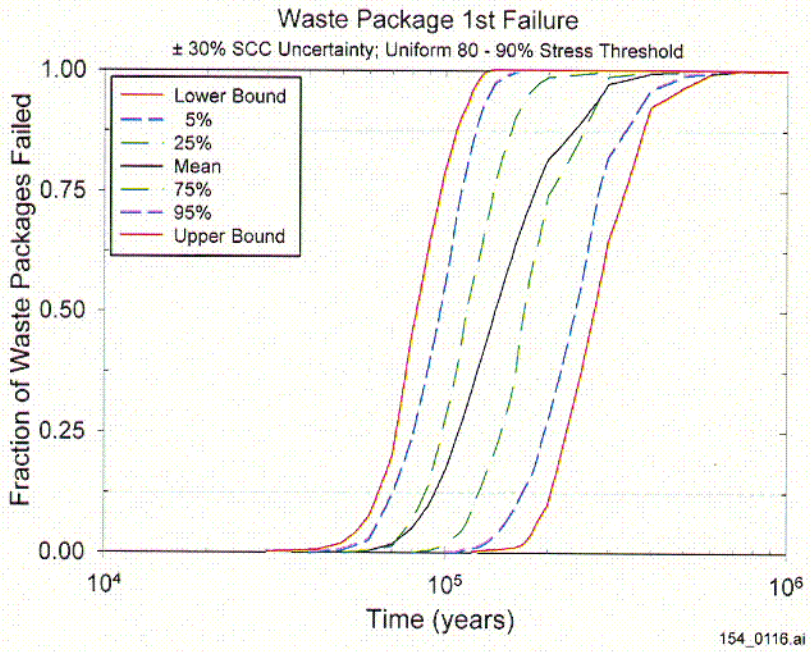

154_0116.ai

Source: Mon 2001 [DIRS 154872].

NOTE: Shown in the figure are the upper and lower bounds, mean, and 95th, 75th, 25th and 5th percentile confidence intervals of the first breach (failure) profile of waste packages with time.

Figure 7.4-10. Waste Package Failure with Time Incorporating the Updated Stress Threshold Uncertainty for Crack Initiation by Stress Corrosion Cracking

C26

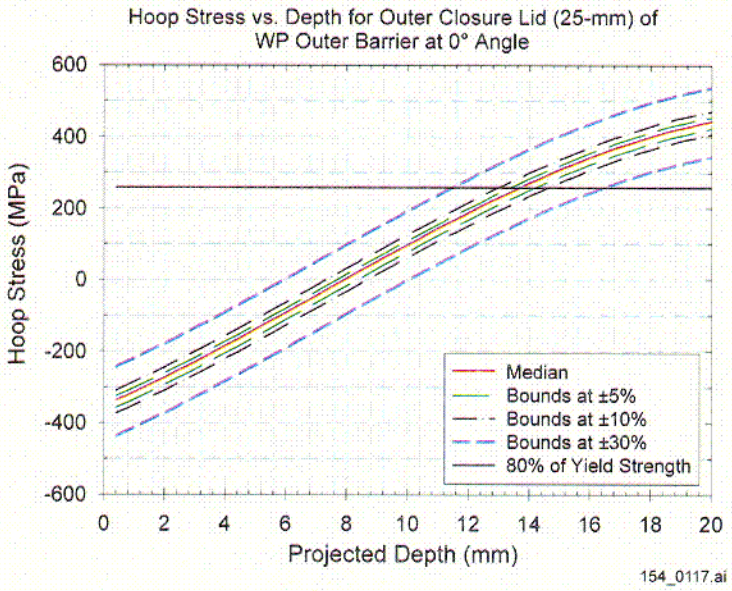

154_0117.ai

Source: DTN: MO0010MWDSUP04.010 [DIRS 152884].

NOTE: Shown in the figure is hoop stress as a function of depth in the Alloy 22 outer closure-lid weld region (25-mm thick) using uncertainty bounds at ±5, 10, and 30 percent of the yield strength, along with the lower bound of the threshold stress (80 percent of the yield strength).

Figure 7.4-11. Hoop Stress versus Depth for Outer Closure-Lid Weld Region of Waste package Outer Barrier

C27

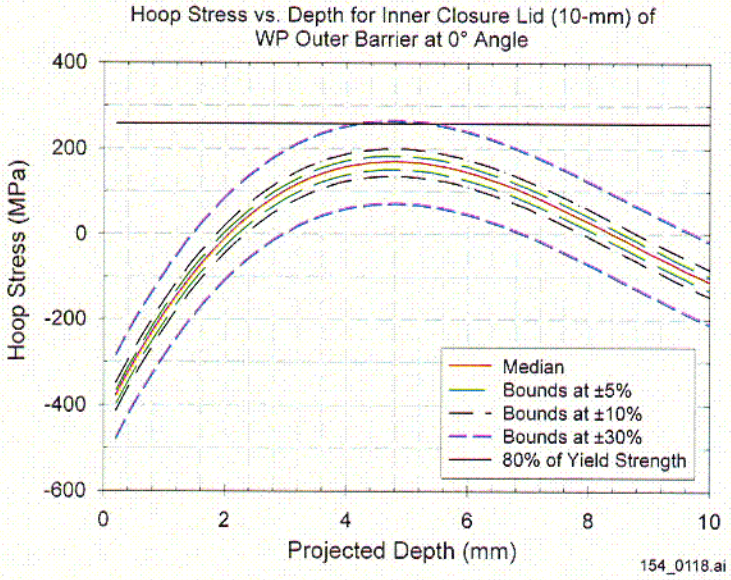

154_0118.ai

Source: DTN: MO0010MWDSUP04.010 [DIRS 152884].

NOTE: Shown in the figure is hoop stress as a function of depth in the Alloy 22 inner closure lid weld region (10-mm thick) using uncertainty bounds at ±5, 10, and 30 percent of the yield strength, along with the lower bound of the threshold stress (80 percent of the yield strength).

Figure 7.4-12. Hoop Stress versus Depth for Inner Closure-Lid Weld Region of Waste Package Outer Barrier for Crack Initiation by Stress Corrosion Cracking

C28

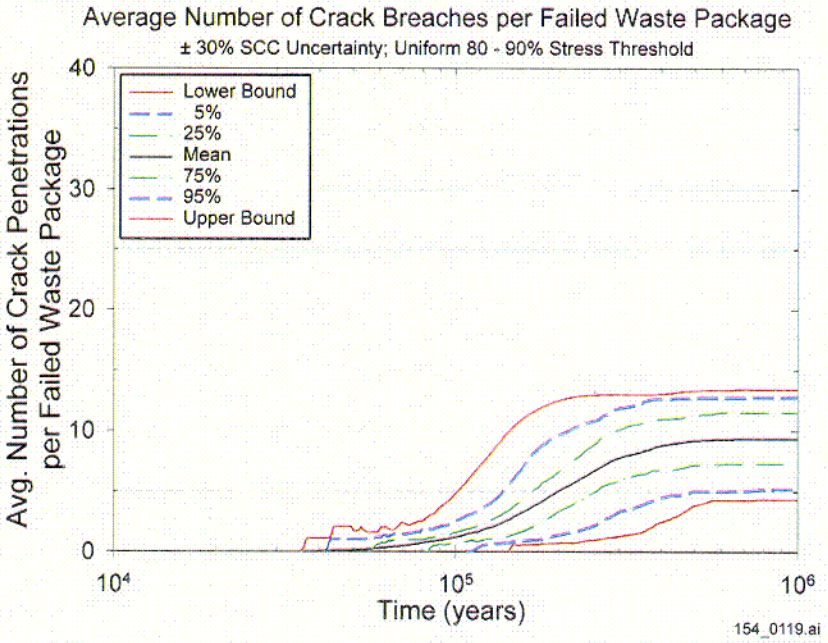

154_0119.ai

Source: Mon 2001 [DIRS 154872].

NOTE: Shown in the figure are the upper and lower bounds, mean, and 95th, 75th, 25th and 5th percentile confidence intervals of the average number of crack breaches per failed waste package with time.

Figure 7.4-13. Average Number of Crack Breaches per Failed Waste Package with Time Incorporating the Updated Stress Threshold Uncertainty for Crack Initiation by Stress Corrosion Cracking

C29

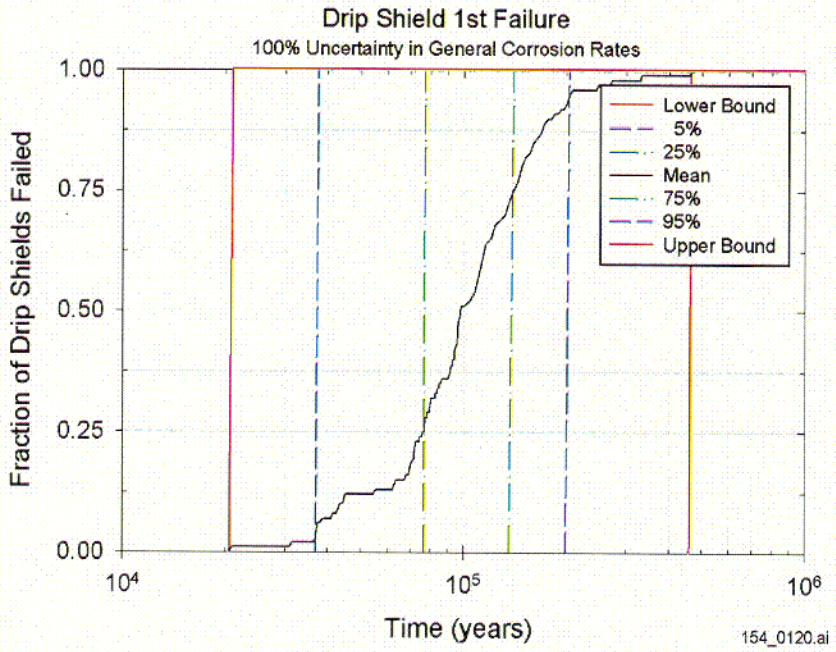

154_0120.ai

Source: Mon 2001 [DIRS 154872].

NOTE: Shown in the figure are the upper and lower bounds, mean, and 95th, 75th, 25th and 5th percentile confidence intervals of the first breach (failure) profile of drip shields with time. The analysis assumes 100 percent uncertainty in the general corrosion rates for the Titanium Grade 7 drip shield.

Figure 7.4-14. Drip Shield Failure with Time Assuming 100 Percent Uncertainty in the General Corrosion Rates

C30

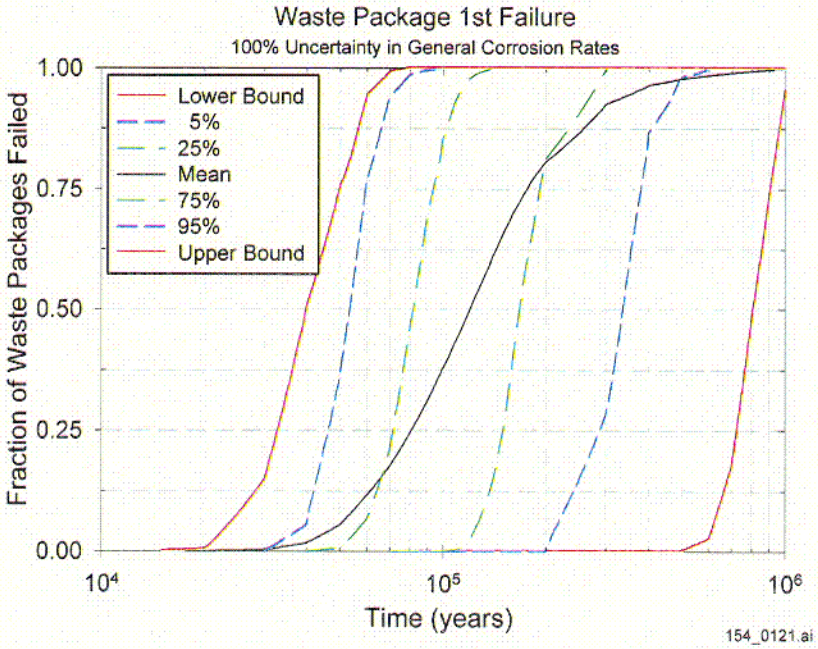

154_0121.ai

Source: Mon 2001 [DIRS 154872].

NOTE: Shown in the figure are the upper and lower bounds, mean, and 95th, 75th, 25th and 5th percentile confidence intervals of the first breach (failure) profile of waste packages with time. The analysis assumes 100 percent uncertainty in the general corrosion rates for the Alloy 22 waste package outer barrier.

Figure 7.4-15. Waste Package First Failure with Time Assuming 100 Percent Uncertainty in the General Corrosion Rates

C31

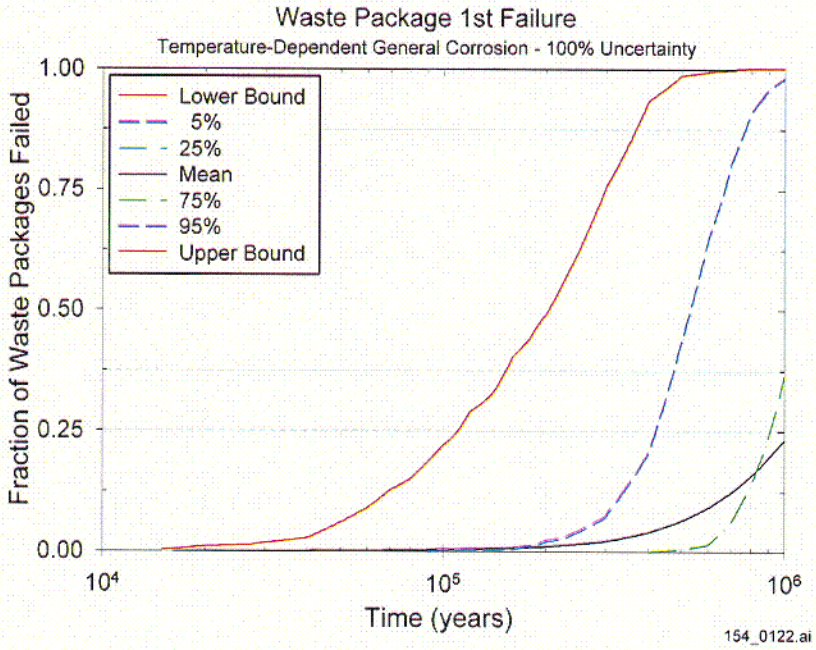

154_0122.ai

Source: Mon 2001 [DIRS 154872].

NOTE: Shown in the figure are the upper and lower bounds, mean, and 95th, 75th, 25th and 5th percentile confidence intervals of the first breach (failure) profile of waste packages with time. The analysis assumes 100 percent uncertainty in the general corrosion rates for the Alloy 22 waste package outer barrier.

Figure 7.4-16. Waste Package Failure with Time Incorporating the Temperature-Dependent Alloy 22 General Corrosion Model I

C32

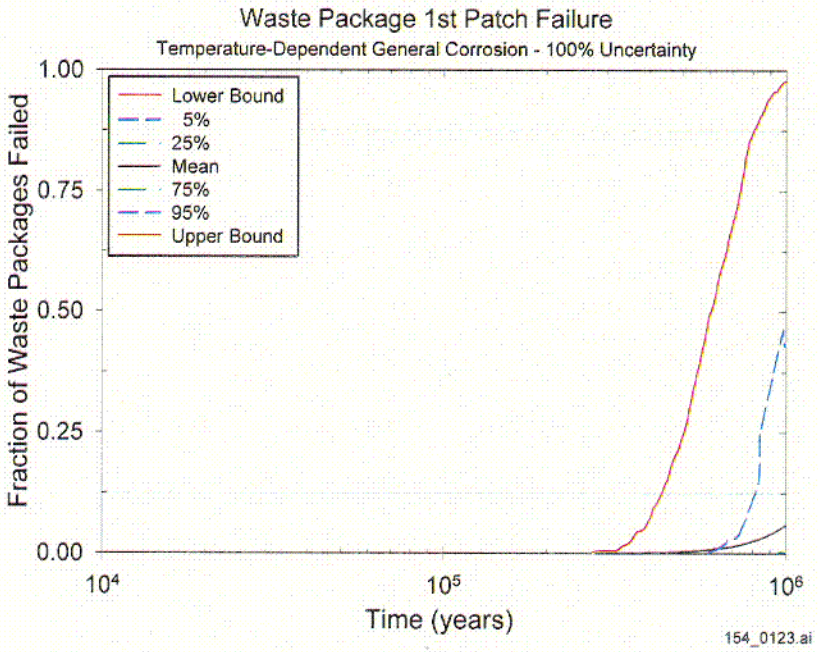

154_0123.ai

Source: Mon 2001 [DIRS 154872].

NOTE: Shown in the figure are the upper and lower bounds, mean, and 95th, 75th, 25th and 5th percentile confidence intervals of the first patch breach profile of waste packages with time. The analysis assumes 100 percent uncertainty in the general corrosion rates for the Alloy 22 waste package outer barrier.

Figure 7.4-17. Waste Package First Patch Failure for the Update Case Incorporating the Temperature-Dependent Alloy 22 General Corrosion Model II

C33

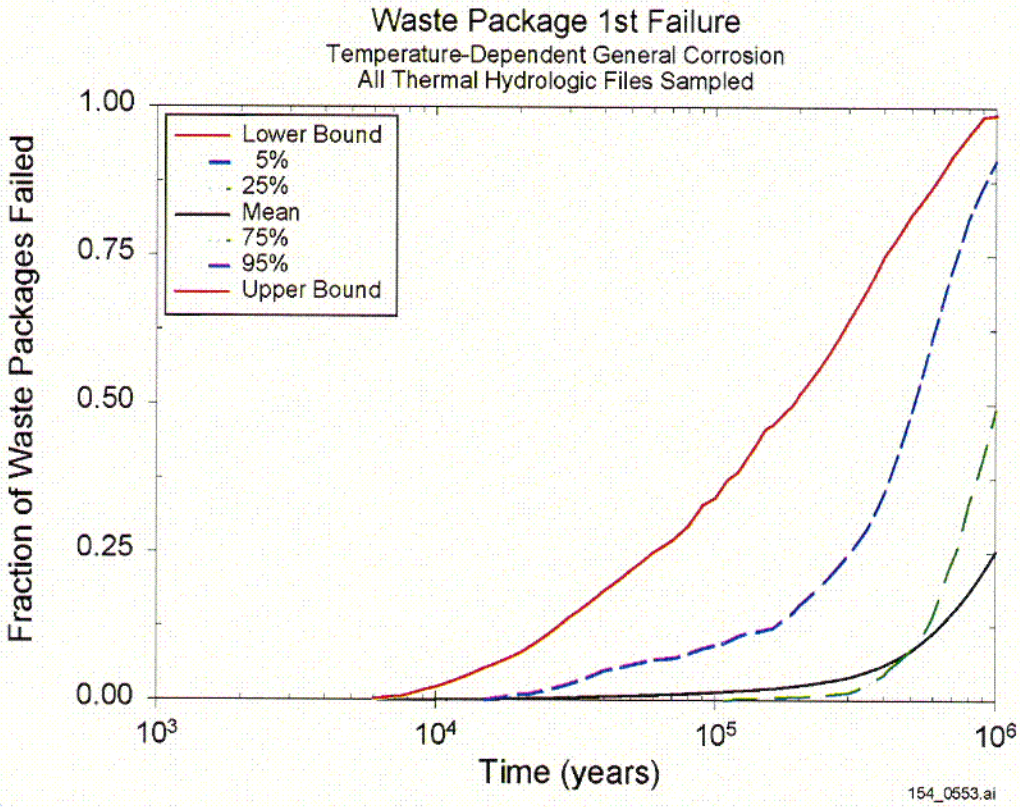

154_0553.ai

Source: Mon 2001 [DIRS 154872].

NOTE: Shown in the figure are the upper and lower bounds, mean, and 95th, 75th, 25th and 5th percentile confidence intervals of the first breach profile of waste packages with time. The analysis assumes 100 percent uncertainty in the general corrosion rates for the Alloy 22 waste package outer barrier. The relative humidity and temperature histories of the waste packages and drip shields included in the analysis are sampled from the temperature and relative humidity histories over the entire repository.

Figure 7.4-18. Waste Package Failure Profile with Time Incorporating the Temperature-Dependent Alloy 22 General Corrosion Model I

C34

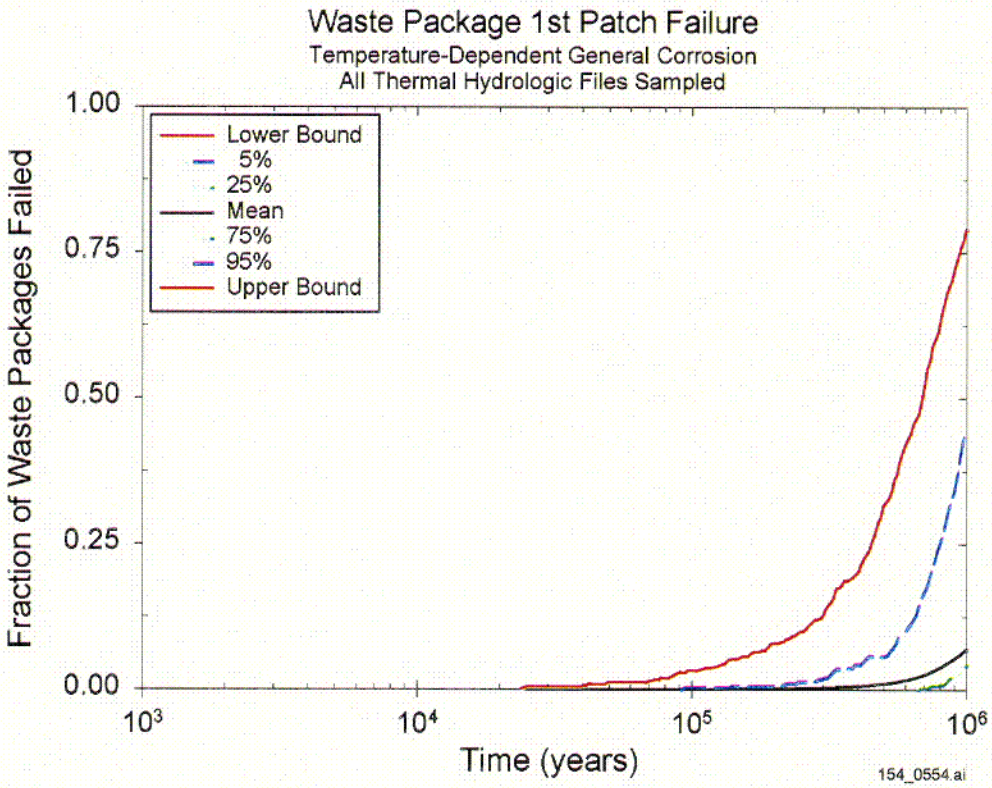

154_0554.ai

Source: Mon 2001 [DIRS 154872].

NOTE: Shown in the figure are the upper and lower bounds, mean, and 95th, 75th, 25th and 5th percentile confidence intervals of the first patch breach profile of waste packages with time. The analysis assumes 100 percent uncertainty in the general corrosion rates for the Alloy 22 waste package outer barrier. The relative humidity and temperature histories of the waste packages and drip shields included in the analysis are sampled from the temperature and relative humidity histories over the entire repository.

Figure 7.4-19. Waste Package First Patch Breach Profile with Time Incorporating the Temperature-Dependent Alloy 22 General Corrosion Model I

C35

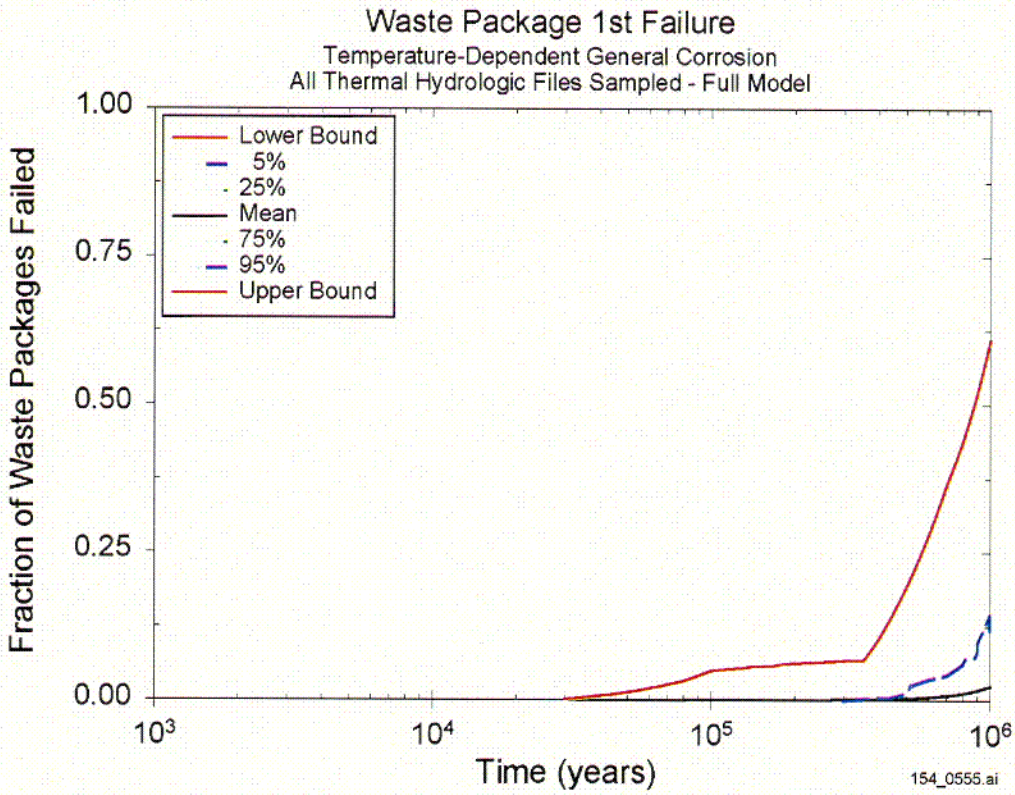

154_0555.ai

Source: Mon 2001 [DIRS 154872].

NOTE: Shown in the figure are the upper and lower bounds, mean, and 95th, 75th, 25th and 5th percentile confidence intervals of the first breach profile of waste packages with time.

Figure 7.4-20. Waste Package Failure Profile with Time for the Integrated Model I

C36

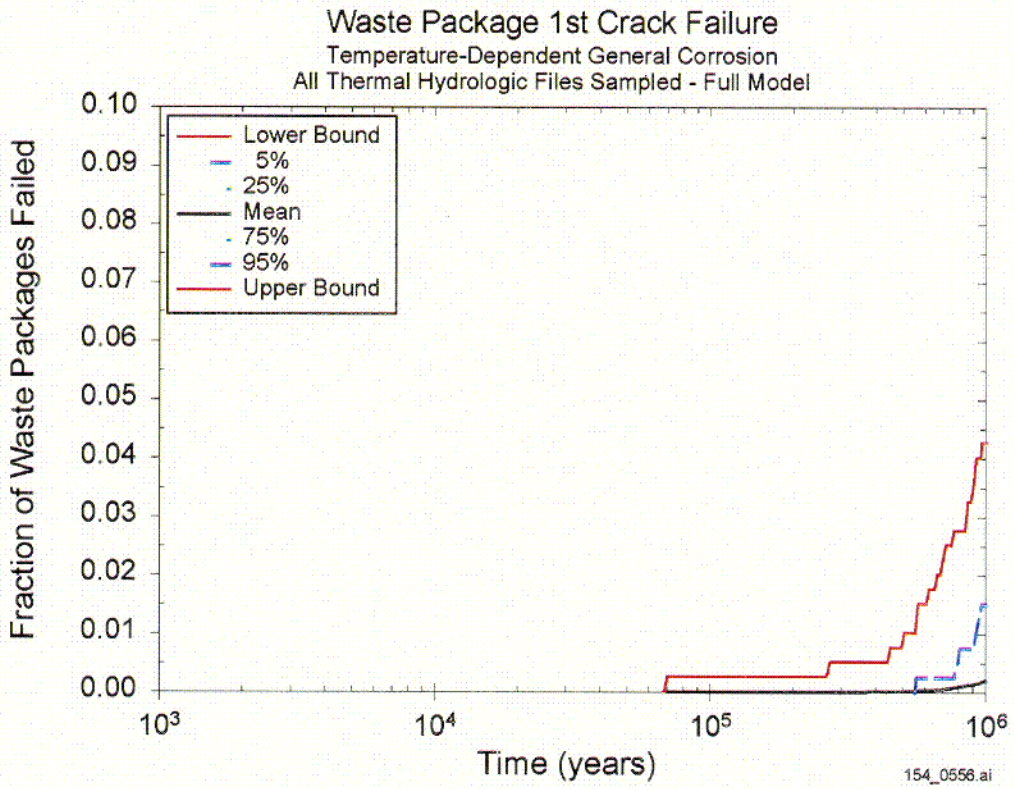

154_0556.ai

Source: Mon 2001 [DIRS 154872].

NOTE: Shown in the figure are the upper and lower bounds, mean, and 95th, 75th, 25th and 5th percentile confidence intervals of the first crack breach profile of waste packages with time.

Figure 7.4-21. Waste Packages First Crack Breach Profile with Time for the Integrated Model I

C37

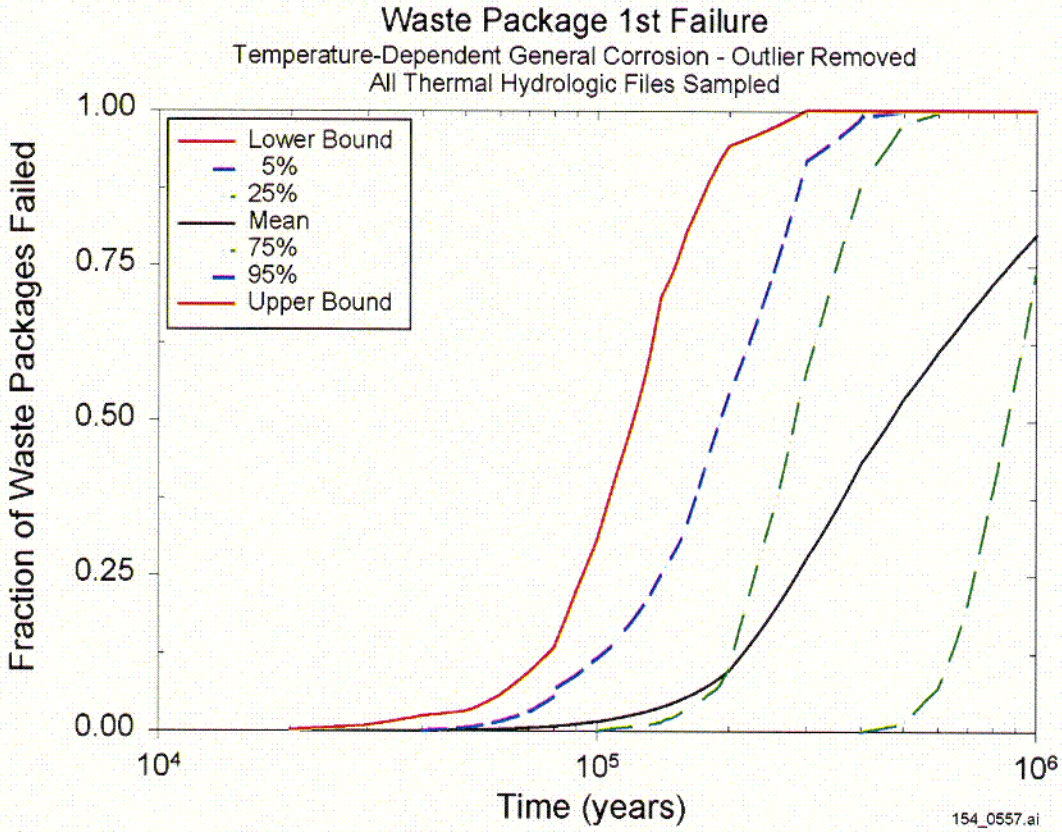

154_0557.ai

Source: Mon 2001 [DIRS 154872].

NOTE: Shown in the figure are the upper and lower bounds, mean, and 95th, 75th, and 25th percentile confidence intervals of the first breach profile of waste packages with time. The analysis assumes 100 percent uncertainty in the general corrosion rates for the Alloy 22 waste package outer barrier. The relative humidity and temperature histories of the waste packages and drip shields included in the analysis are sampled from the temperature and relative humidity histories over the entire repository.

Figure 7.4-22. Waste Package Failure Profile with Time Incorporating the Temperature-Dependent Alloy 22 General Corrosion Model II

C38

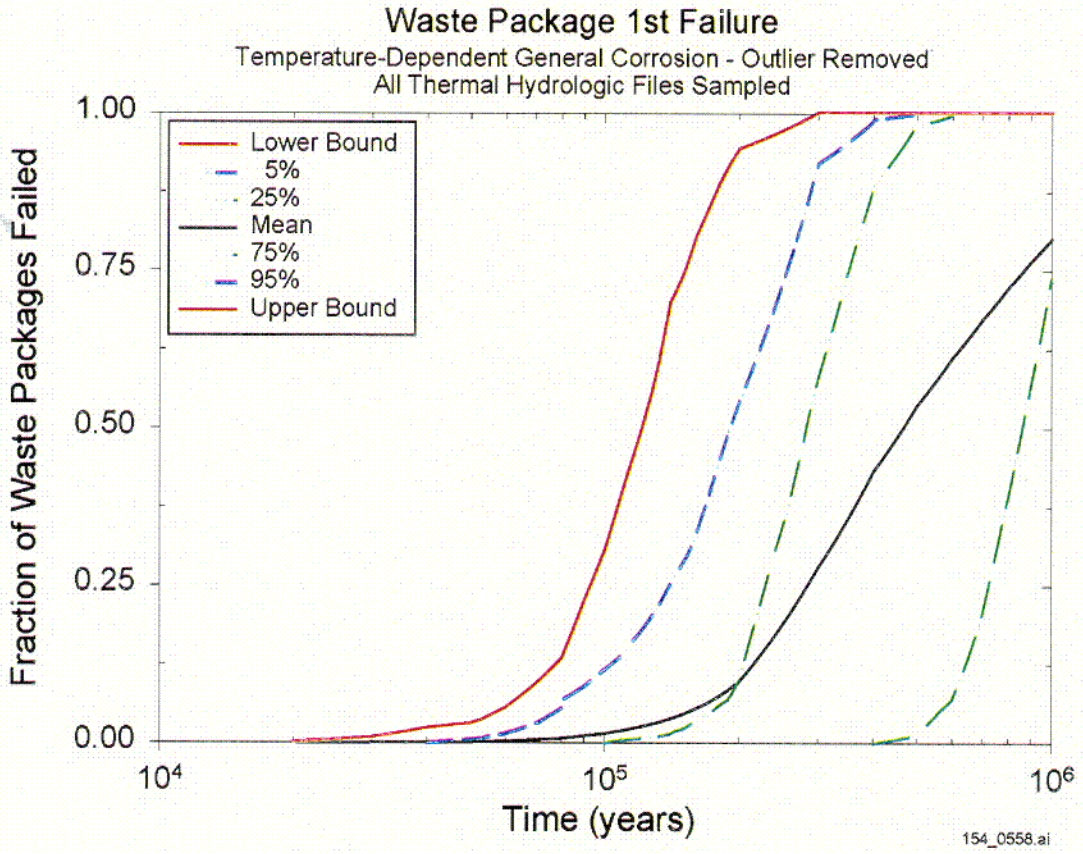

154_0558.ai

Source: Mon 2001 [DIRS 154872].

NOTE: Shown in the figure are the upper and lower bounds, mean, and 95th, 75th and 25th percentile confidence intervals of the first patch breach profile of waste packages with time. The analysis assumes 100 percent uncertainty in the general corrosion rates for the Alloy 22 waste package outer barrier. The relative humidity and temperature histories of the waste packages and drip shields included in the analysis are sampled from the temperature and relative humidity histories over the entire repository.

Figure 7.4-23. Waste Package First Patch Breach Profile with Time Incorporating the Temperature-Dependent Alloy 22 General Corrosion Model II

C39

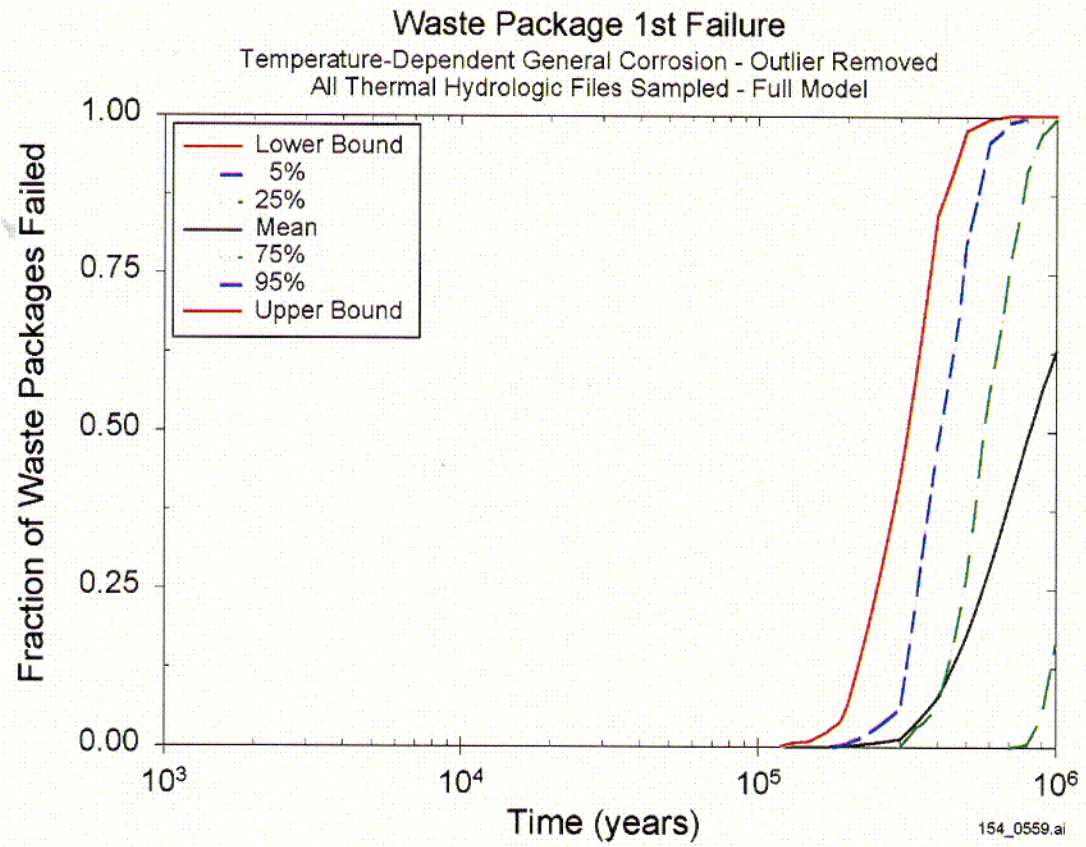

154_0559.ai

Source: Mon 2001 [DIRS 154872].

NOTE: Shown in the figure are the upper and lower bounds, mean, and 95th, 75th and 25th percentile confidence intervals of the first breach profile of waste packages with time.

Figure 7.4-24. Waste Package Failure Profile with Time for the Integrated Model II

C40

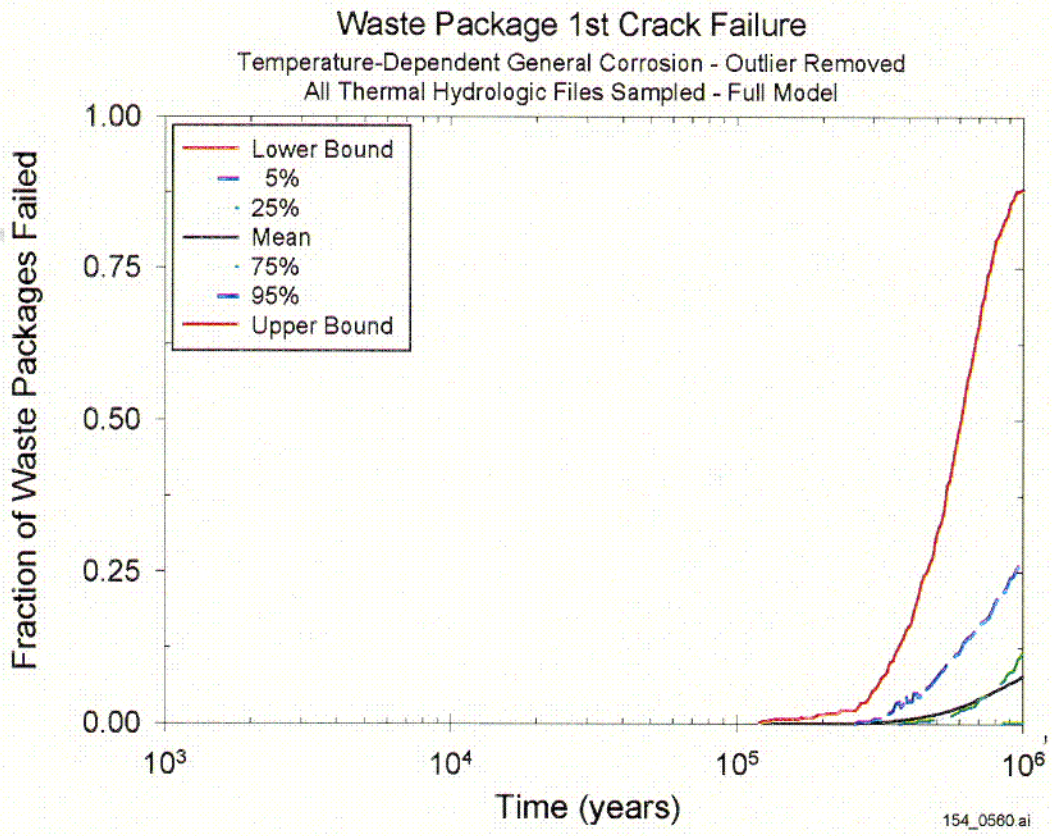

154_0560.ai

Source: Mon 2001 [DIRS 154872].

NOTE: Shown in the figure are the upper and lower bounds, mean, and 95th, 75th and 25th percentile confidence intervals of the first crack breach profile of waste packages with time.

Figure 7.4-25. Waste Packages First Crack Breach Profile with Time for the Integrated Model II

C41

INTENTIONALLY LEFT BLANK

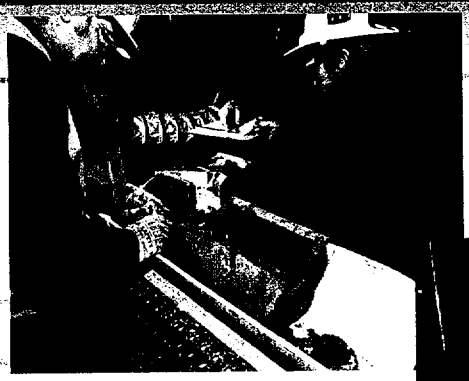

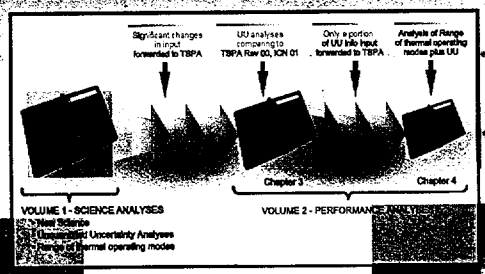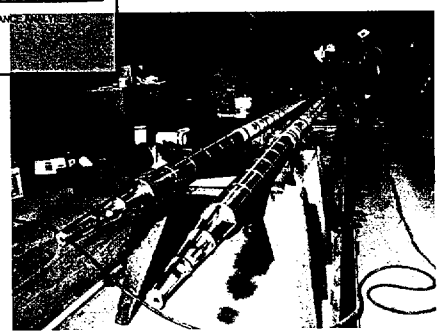
Significant changes in input forwarded to TSPA
UU analyses comparing to TSPA Rev 00, ICN 01
Only a portion of UU info input forwarded to TSPA
Analysis of Range of thermal operating modes plus UU
Chapter 3
Chapter 4
VOLUME 1 - SCIENCE ANALYSES
VOLUME 2 - PERFORMANCE
Uncertainty Analyses
Range of thermal operating modes